Vietnam Journal of Mechanics, Vol. 45, No. 1 (2023), pp. 36 – 59
DOI: https://doi.org/10.15625/0866-7136/17552

STATIC AND VIBRATION ANALYSIS OF FUNCTIONALLY GRADED MICROPLATE WITH POROSITIES BASED ON HIGHER-ORDER SHEAR DEFORMATION AND MODIFIED STRAIN GRADIENT THEORY

Van-Thien Tran[1], **Van-Hau Nguyen**[1,*], **Trung-Kien Nguyen**[2], **Thuc P. Vo**[3]
[1]*Faculty of Civil Engineering, Ho Chi Minh City University of Technology an Education, 1 Vo Van Ngan street, Thu Duc City, Ho Chi Minh City, Vietnam*
[2]*CIRTech Institute, HUTECH University, 475A Dien Bien Phu street, Binh Thanh district, Ho Chi Minh City, Vietnam*
[3]*School of Computing, Engineering and Mathematical Sciences, La Trobe University, Bundoora, VIC 3086, Australia*
[*]E-mail: haunv@hcmute.edu.vn

Received: 16 November 2022 / Published online: 01 March 2023

Abstract. Based on fundamental equations of the elasticity theory, a unified higher-order shear deformation theory is developed for bending and free vibration analysis of functionally graded (FG) microplates with porosities. The modified strain gradient theory is employed to capture the size effects. Bi-directional series with hybrid shape functions are used to solve the problems. Several important effects including thickness-to-material length scale parameters, side-to-thickness ratio, and boundary conditions on the deflections and natural frequencies of FG porous microplates are investigated.

Keywords: bending, vibration, functionally graded microplates, porosity, modified strain gradient theory, higher-order shear deformation theory.

1. INTRODUCTION

Microstructures have been applied in many engineering fields such as atomic force microscopes, microelectromechanical systems and nano-electromechanical systems [1,2]. The recent development of functionally graded porous (FGP) materials led to a potential application, it hence requires advanced computational methods and models especially at microscales. The study on static and dynamic responses of FGP plates and shells has attracted a number of researches with various computational methods and

models [3–14], however, those classical elasticity models could not accurately predict responses of microstructures. Therefore, advanced computations theories with material length scale parameters (MLSPs) have been developed with different approaches. A number of researches has been performed for FGP microplates in which the modified coupled stress theory (MCT) are mostly used. By considering the rotation gradient in constitutive equations, the MCT with only one MLSP is known as the simplest theory accounted for the size effects [15]. Owing to its simplicity, many size-dependent FGP microplate models with different shear deformation theories based on the MCT have been developed [16–18]. By adding strain gradients into the strain energy, the modified strain gradient theory (MST) with three MLSPs was proposed by Lam et al. [19] based on the classical strain gradient theory of Mindlin [20, 21]. This theory is more general than the MCT and it can be recovered by the MST if the effects of dilatation and deviatoric stretch gradients are neglected. By its advantages, the MST has been developed for static and dynamic of FG microplates [17,22–25]. A brief literature review showed that although many studies have been performed for static and dynamic analysis of FGP microplates using different existing shear deformation plate theories and MCT, however, the investigation based on the MST is still limited, this gap needs to be studied further.

The objective of this paper is to develop a unified framework of higher-order shear deformation theory (HSDT) for static and free vibration analyses of FGP microplates based on the MST. Hamilton's principle is used to derive the governing equations of motion, which are then solved by bi-directional series-type solutions with hybrid shape functions. Several important effects such as, thickness-to-MLSP ratio, side-to-thickness ratio, boundary conditions on the deflections and natural frequencies of FGP microplates are investigated. Some results given in this paper can be used for the future references.

2. THEORETICAL FORMULATION

Consider a rectangular FGP microplate in the coordinate system (x_1, x_2, x_3) with sides $a \times b$ and thickness h. It is supposed that the FGP microplates are composed of a metal-ceramic mixture and porosity density whose effective material properties can be approximated by the following expressions [3, 26, 27]

$$P\left(x_3\right) = \left(P_c - P_m\right)\left(\frac{2x_3 + h}{2h}\right)^p + P_m - \frac{\beta}{2}\left(P_c + P_m\right), \tag{1}$$

where P_c and P_m are the properties of ceramic and metal materials, such as Young's modulus E, mass density ρ, Poisson's ratio ν; β is the porosity volume fraction, $0 \leq \beta \ll 1$; p is the power-law index which is positive and $x_3 \in [-h/2, h/2]$.

2.1. Modified strain gradient theory (MST)

The total potential energy of the FGP microplate is obtained by

$$\Pi = \Pi_U + \Pi_V - \Pi_K, \tag{2}$$

where Π_U, Π_V, Π_K are the strain energy, work done by external forces and kinetic energy of the FGP microplates, respectively. Based on the MST, the strain energy of the system Π_U is given by

$$\Pi_U = \int_V (\boldsymbol{\sigma}\boldsymbol{\varepsilon} + \mathbf{p}\xi + \boldsymbol{\tau}\boldsymbol{\eta} + \mathbf{m}\boldsymbol{\chi}) \mathrm{d}V, \tag{3}$$

where $\boldsymbol{\varepsilon}, \boldsymbol{\chi}, \boldsymbol{\xi}, \boldsymbol{\eta}$ are strains, symmetric rotation gradients, dilatation gradient and deviation stretch gradient, respectively; $\boldsymbol{\sigma}$ is Cauchy stress; $\mathbf{m}, \mathbf{p}, \boldsymbol{\tau}$ are high-order stresses corresponding with strain gradients $\boldsymbol{\chi}, \boldsymbol{\xi}, \boldsymbol{\eta}$, respectively. The components of strain ε_{ij} and strain gradients $\xi_i, \eta_{ijk}, \chi_{ij}$ are defined as follows

$$\varepsilon_{ij} = \frac{1}{2}\left(u_{i,j} + u_{j,i}\right), \quad \xi_i = \varepsilon_{mm,i}, \quad \chi_{ij} = \frac{1}{4}\left(u_{n,mj}e_{imn} + u_{n,mi}e_{jmn}\right), \tag{4a}$$

$$\eta_{ijk} = \frac{1}{3}\left(\varepsilon_{jk,i} + \varepsilon_{ki,j} + \varepsilon_{ij,k}\right) - \frac{1}{15}\left[\left(\xi_k + 2\varepsilon_{mk,m}\right)\delta_{ij} + \left(\xi_i + 2\varepsilon_{mi,m}\right)\delta_{jk} + \left(\xi_j + 2\varepsilon_{mj,m}\right)\delta_{ki}\right], \tag{4b}$$

where δ_{ij}, e_{imn} are Knonecker delta and permutation symbol, respectively; the comma in subscript is used to indicate the partial derivative with respect to the followed variable. The components of stress are calculated from constitutive as follows

$$\sigma_{ij} = \lambda\varepsilon_{kk}\delta_{ij} + 2\mu\varepsilon_{ij}, \quad m_{ij} = 2\mu l_1^2\chi_{ij}, \quad p_j = 2\mu l_2^2\xi_j, \quad \tau_{ijk} = 2\mu l_3^2\eta_{ijk}, \tag{5}$$

where λ, μ are Lamé constants; l_1, l_2, l_3 are three MLSPs.

The work done by a transverse load q of the FGP microplates is given by

$$\Pi_V = -\int_A q u_3^0 \mathrm{d}A. \tag{6}$$

The kinetic energy of the FGP microplates Π_K is expressed by

$$\Pi_K = \frac{1}{2}\int_V \rho\left(x_3\right)\left(\dot{u}_1^2 + \dot{u}_2^2 + \dot{u}_3^2\right)\mathrm{d}V. \tag{7}$$

2.2. Unified kinematics of FGP microplates

A general HSDT kinematic of FGP microplates is derived from [28,29] as follows

$$u_1\left(x_1, x_2, x_3\right) = u_1^0\left(x_1, x_2\right) + \Phi_1\left(x_3\right)u_{3,1}^0 + \Phi_2\left(x_3\right)\varphi_1\left(x_1, x_2\right), \tag{8a}$$

$$u_2\left(x_1, x_2, x_3\right) = u_2^0\left(x_1, x_2\right) + \Phi_1\left(x_3\right)u_{3,2}^0 + \Phi_2\left(x_3\right)\varphi_2\left(x_1, x_2\right), \tag{8b}$$

$$u_3\left(x_1, x_2, x_3\right) = u_3^0\left(x_1, x_2\right), \tag{8c}$$

where $\Phi_1\left(x_3\right) = H^s\Psi\left(x_3\right) - x_3, \Phi_2\left(x_3\right) = H^s\Psi\left(x_3\right)$; u_1^0, u_2^0 and u_3^0, φ_1, φ_2 are membrane and transverse displacements, rotations around the x_2- and x_1-axis at the mid-surface of FGP microplates, respectively; H^s is the transverse shear stiffness of the FGP microplates; $\Psi\left(x_3\right) = \int_0^{x_3} \frac{f_{,3}}{\mu\left(x_3\right)} dx_3$ is a shear function; $\mu\left(x_3\right) = \frac{E\left(x_3\right)}{2\left(1+\nu\right)}$ is the shear modulus; $f\left(x_3\right)$ is a higher-order term whose first derivative satisfies the free-stress boundary condition

at the top and bottom surfaces of the plates, i.e. $f_{,3}\left(x_3 = \pm\frac{h}{2}\right) = 0$. Substituting Eq. (8) into the strains and strain gradients in Eq. (4), the strains are obtained as follows

$$\boldsymbol{\varepsilon}^{(i)} = \boldsymbol{\varepsilon}^{(0)} + \Phi_1(x_3)\,\boldsymbol{\varepsilon}^{(1)} + \Phi_2(x_3)\,\boldsymbol{\varepsilon}^{(2)}, \quad \boldsymbol{\varepsilon}^{(s)} = \Phi_3(x_3)\,\boldsymbol{\varepsilon}^{(3)}, \tag{9}$$

where $\Phi_3(x_3) = H^s\Psi_{,3}$ with $\Psi_{,3}(x_3) = \dfrac{f_{,3}(x_3)}{\mu(x_3)}$ and,

$$\begin{aligned}
\boldsymbol{\varepsilon}^{(0)} &= \begin{Bmatrix} \varepsilon_{11}^{(0)} \\ \varepsilon_{22}^{(0)} \\ \gamma_{12}^{(0)} \end{Bmatrix} = \begin{Bmatrix} u_{1,1}^0 \\ u_{2,2}^0 \\ u_{1,2}^0 + u_{2,1}^0 \end{Bmatrix}, \quad \boldsymbol{\varepsilon}^{(1)} = \begin{Bmatrix} \varepsilon_{11}^{(1)} \\ \varepsilon_{22}^{(1)} \\ \gamma_{12}^{(1)} \end{Bmatrix} = \begin{Bmatrix} u_{3,11}^0 \\ u_{3,22}^0 \\ 2u_{3,12}^0 \end{Bmatrix}, \\
\boldsymbol{\varepsilon}^{(2)} &= \begin{Bmatrix} \varepsilon_{11}^{(2)} \\ \varepsilon_{22}^{(2)} \\ \gamma_{12}^{(2)} \end{Bmatrix} = \begin{Bmatrix} \varphi_{1,1} \\ \varphi_{2,2} \\ \varphi_{1,2} + \varphi_{2,1} \end{Bmatrix}, \quad \boldsymbol{\varepsilon}^{(3)} = \begin{Bmatrix} \gamma_{13}^{(0)} \\ \gamma_{23}^{(0)} \end{Bmatrix} = \begin{Bmatrix} \varphi_1 + u_{3,1}^0 \\ \varphi_2 + u_{3,2}^0 \end{Bmatrix}.
\end{aligned} \tag{10}$$

The non-zero components of dilatation gradients $\boldsymbol{\xi} = \begin{bmatrix} \xi_1 & \xi_2 & \xi_3 \end{bmatrix}^T$ are given by

$$\boldsymbol{\xi} = \boldsymbol{\xi}^{(0)} + \Phi_1\boldsymbol{\xi}^{(1)} + \Phi_2\boldsymbol{\xi}^{(2)} + \Phi_{1,3}\boldsymbol{\xi}^{(3)} + \Phi_{2,3}\boldsymbol{\xi}^{(4)}. \tag{11}$$

The non-zero components of deviatoric stretch gradients $\boldsymbol{\eta}_{ijk}$ are given by

$$\boldsymbol{\eta} = \boldsymbol{\eta}^{(0)} + \Phi_1\boldsymbol{\eta}^{(1)} + \Phi_2\boldsymbol{\eta}^{(2)} + \Phi_3\boldsymbol{\eta}^{(3)} + \Phi_{1,3}\boldsymbol{\eta}^{(4)} + \Phi_{2,3}\boldsymbol{\eta}^{(5)} + \Phi_{3,3}\boldsymbol{\eta}^{(6)}, \tag{12}$$

where $\boldsymbol{\eta}^T = \begin{bmatrix} \eta_{111} & \eta_{222} & \eta_{333} & 3\eta_{331} & 3\eta_{332} & 3\eta_{221} & 3\eta_{112} & 3\eta_{113} & 3\eta_{223} & 6\eta_{123} \end{bmatrix}$.

The rotation gradients are expressed as follows

$$\boldsymbol{\chi} = \boldsymbol{\chi}^{(0)} + \Phi_{1,3}\boldsymbol{\chi}^{(1)} + \Phi_{2,3}\boldsymbol{\chi}^{(2)} + \Phi_{1,33}\boldsymbol{\chi}^{(3)} + \Phi_{2,33}\boldsymbol{\chi}^{(4)} + \Phi_2\boldsymbol{\chi}^{(5)}, \tag{13}$$

with $\boldsymbol{\chi}^T = \begin{bmatrix} \chi_{11} & \chi_{22} & 2\chi_{12} & \chi_{33} & 2\chi_{13} & 2\chi_{23} \end{bmatrix}$. The components of $\boldsymbol{\xi}, \boldsymbol{\eta}, \boldsymbol{\chi}$ can be seen more details in Appendix A. Furthermore, the stresses and strains of FGP microplates are related by constitutive equations as follows

$$\begin{aligned}
\boldsymbol{\sigma}^{(i)} &= \begin{Bmatrix} \sigma_{11} \\ \sigma_{22} \\ \sigma_{12} \end{Bmatrix} = \begin{bmatrix} Q_{11} & Q_{12} & 0 \\ Q_{12} & Q_{22} & 0 \\ 0 & 0 & Q_{66} \end{bmatrix} \begin{Bmatrix} \varepsilon_{11} \\ \varepsilon_{22} \\ \gamma_{12} \end{Bmatrix} = \mathbf{Q}_\varepsilon^{(i)}\boldsymbol{\varepsilon}^{(i)}, \\
\boldsymbol{\sigma}^{(o)} &= \begin{Bmatrix} \sigma_{13} \\ \sigma_{23} \end{Bmatrix} = \begin{bmatrix} Q_{55} & 0 \\ 0 & Q_{44} \end{bmatrix} \begin{Bmatrix} \gamma_{13} \\ \gamma_{23} \end{Bmatrix} = \mathbf{Q}_\varepsilon^{(o)}\boldsymbol{\varepsilon}^{(s)},
\end{aligned} \tag{14a}$$

$$\begin{aligned}
\mathbf{m} &= \begin{Bmatrix} m_{11} \\ m_{22} \\ m_{12} \\ m_{33} \\ m_{23} \\ m_{13} \end{Bmatrix} = 2\mu l_1^2 \begin{bmatrix} 1 & 0 & 0 & 0 & 0 & 0 \\ 0 & 1 & 0 & 0 & 0 & 0 \\ 0 & 0 & 1 & 0 & 0 & 0 \\ 0 & 0 & 0 & 1 & 0 & 0 \\ 0 & 0 & 0 & 0 & 1 & 0 \\ 0 & 0 & 0 & 0 & 0 & 1 \end{bmatrix} \begin{Bmatrix} \chi_{11} \\ \chi_{22} \\ \chi_{12} \\ \chi_{33} \\ \chi_{23} \\ \chi_{13} \end{Bmatrix} = \alpha_{\chi_6}\mathbf{I}_{6\times 6}\boldsymbol{\chi}, \\
\mathbf{p} &= \begin{Bmatrix} p_1 \\ p_2 \\ p_3 \end{Bmatrix} = 2\mu l_2^2 \begin{bmatrix} 1 & 0 & 0 \\ 0 & 1 & 0 \\ 0 & 0 & 1 \end{bmatrix} \begin{Bmatrix} \xi_1 \\ \xi_2 \\ \xi_3 \end{Bmatrix} = \alpha_\xi\mathbf{I}_{3\times 3}\boldsymbol{\xi},
\end{aligned} \tag{14b}$$

$$\boldsymbol{\tau}=\left\{\begin{array}{c}\tau_{111}\\ \tau_{222}\\ \tau_{112}\\ \tau_{221}\\ \tau_{331}\\ \tau_{332}\\ \tau_{333}\\ \tau_{113}\\ \tau_{223}\\ \tau_{123}\end{array}\right\}=2\mu_3^2\left[\begin{array}{cccccccccc}1&0&0&0&0&0&0&0&0&0\\ 0&1&0&0&0&0&0&0&0&0\\ 0&0&1&0&0&0&0&0&0&0\\ 0&0&0&1&0&0&0&0&0&0\\ 0&0&0&0&1&0&0&0&0&0\\ 0&0&0&0&0&1&0&0&0&0\\ 0&0&0&0&0&0&1&0&0&0\\ 0&0&0&0&0&0&0&1&0&0\\ 0&0&0&0&0&0&0&0&1&0\\ 0&0&0&0&0&0&0&0&0&1\end{array}\right]\left\{\begin{array}{c}\eta_{111}\\ \eta_{222}\\ \eta_{112}\\ \eta_{221}\\ \eta_{331}\\ \eta_{332}\\ \eta_{333}\\ \eta_{113}\\ \eta_{223}\\ \eta_{123}\end{array}\right\}=\alpha_\eta\mathbf{I}_{10\times10}\boldsymbol{\eta}, \quad (14c)$$

where $\alpha_\chi=2\mu l_1^2,\alpha_\xi=2\mu l_2^2,\alpha_\eta=2\mu l_3^2$, and

$$Q_{11}=\frac{E\left(x_3\right)}{1-v^2},\ Q_{22}=\frac{E\left(x_3\right)}{1-v^2},\ Q_{12}=\frac{vE\left(x_3\right)}{1-v^2},\ Q_{44}=Q_{55}=Q_{66}=\mu=\frac{E\left(x_3\right)}{2(1+v)}. \quad (15)$$

2.3. Energy principle

In order to derive the equation of motion, Hamilton's principle is used

$$\int_{t_1}^{t_2}\left(\delta\Pi_U+\delta\Pi_V-\delta\Pi_K\right)\mathrm{d}t=0, \quad (16)$$

where $\delta\Pi_U,\delta\Pi_V,\delta\Pi_K$ are the variations of strain energy, work done by external force and kinetic energy, respectively. The variation of the strain energy of FGP microplates derived from Eq. (3) as follows

$$\begin{aligned}\delta\Pi_U=&\int_A(\boldsymbol{\sigma}\delta\boldsymbol{\varepsilon}+\mathbf{p}\delta\boldsymbol{\xi}+\boldsymbol{\tau}\delta\boldsymbol{\eta}+\mathbf{m}\delta\boldsymbol{\chi})\mathrm{d}A=\int_A\Big[\mathbf{M}_\varepsilon^{(0)}\delta\boldsymbol{\varepsilon}^{(0)}+\mathbf{M}_\varepsilon^{(1)}\delta\boldsymbol{\varepsilon}^{(1)}+\mathbf{M}_\varepsilon^{(2)}\delta\boldsymbol{\varepsilon}^{(2)}\\ &+\mathbf{M}_\varepsilon^{(3)}\delta\boldsymbol{\varepsilon}^{(3)}+\mathbf{M}_\xi^{(0)}\delta\boldsymbol{\xi}^{(0)}+\mathbf{M}_\xi^{(1)}\delta\boldsymbol{\xi}^{(1)}+\mathbf{M}_\xi^{(2)}\delta\boldsymbol{\xi}^{(2)}+\mathbf{M}_\xi^{(3)}\delta\boldsymbol{\xi}^{(3)}+\mathbf{M}_\xi^{(4)}\delta\boldsymbol{\xi}^{(4)}\\ &+\mathbf{M}_\chi^{(0)}\delta\boldsymbol{\chi}^{(0)}+\mathbf{M}_\chi^{(1)}\delta\boldsymbol{\chi}^{(1)}+\mathbf{M}_\chi^{(2)}\delta\boldsymbol{\chi}^{(2)}+\mathbf{M}_\chi^{(3)}\delta\chi^{(3)}+\mathbf{M}_\chi^{(4)}\delta\boldsymbol{\chi}^{(4)}+\mathbf{M}_\chi^{(5)}\delta\boldsymbol{\chi}^{(5)}\\ &+\mathbf{M}_\eta^{(0)}\delta\boldsymbol{\eta}^{(0)}+\mathbf{M}_\eta^{(1)}\delta\boldsymbol{\eta}^{(1)}+\mathbf{M}_\eta^{(2)}\delta\boldsymbol{\eta}^{(2)}+\mathbf{M}_\eta^{(3)}\delta\boldsymbol{\eta}^{(3)}+\mathbf{M}_\eta^{(4)}\delta\boldsymbol{\eta}^{(4)}+\mathbf{M}_\eta^{(5)}\delta\boldsymbol{\eta}^{(5)}+\mathbf{M}_\eta^{(6)}\delta\boldsymbol{\eta}^{(6)}\Big]\mathrm{d}A,\end{aligned} \quad (17)$$

where the stress resultants are given by

$$\left(\mathbf{M}_\varepsilon^{(0)},\mathbf{M}_\varepsilon^{(1)},\mathbf{M}_\varepsilon^{(2)}\right)=\int_{-h/2}^{h/2}\left(1,\Phi_1,\Phi_2\right)\boldsymbol{\sigma}^{(i)}\mathrm{d}x_3,\quad \mathbf{M}_\varepsilon^{(3)}=\int_{-h/2}^{h/2}\Phi_3\boldsymbol{\sigma}^{(o)}\mathrm{d}x_3, \quad (18a)$$

$$\left(\mathbf{M}_\xi^{(0)},\mathbf{M}_\xi^{(1)},\mathbf{M}_\xi^{(2)},\mathbf{M}_\xi^{(3)},\mathbf{M}_\xi^{(4)}\right)=\int_{-h/2}^{h/2}\left(1,\Phi_1,\Phi_2,\Phi_{1,3},\Phi_{2,3}\right)\mathbf{p}\mathrm{d}x_3, \quad (18b)$$

$$\left(\mathbf{M}_\chi^{(0)},\mathbf{M}_\chi^{(1)},\mathbf{M}_\chi^{(2)},\mathbf{M}_\chi^{(3)},\mathbf{M}_\chi^{(4)},\mathbf{M}_\chi^{(5)}\right)=\int_{-h/2}^{h/2}\left(1,\Phi_{1,3},\Phi_{2,3},\Phi_{1,33},\Phi_{2,33},\Phi_2\right)\mathbf{m}\mathrm{d}x_3, \quad (18c)$$

$$\left(\mathbf{M}_\eta^{(0)},\mathbf{M}_\eta^{(1)},\mathbf{M}_\eta^{(2)},\mathbf{M}_\eta^{(3)},\mathbf{M}_\eta^{(4)},\mathbf{M}_\eta^{(5)},\mathbf{M}_\eta^{(6)}\right)=\int_{-h/2}^{h/2}\left(1,\Phi_1,\Phi_2,\Phi_3,\Phi_{1,3},\Phi_{2,3},\Phi_{3,3}\right)\boldsymbol{\eta}\mathrm{d}x_3. \quad (18d)$$

These stress resultants can be expressed in terms of the strains and its gradients (see Appendix B for more details).

The variation of work done by transverse loads derived from Eq. (6) is given by

$$\delta\Pi_V = -\int_A q\delta u_3^0 \mathrm{d}A. \tag{19}$$

The variation of kinetic energy $\delta\Pi_K$ derived from Eq. (7) is calculated by

$$\begin{aligned}\delta\Pi_K = \frac{1}{2}\int_V \rho\left(\dot{u}_1\delta\dot{u}_1 + \dot{u}_2\delta\dot{u}_2 + \dot{u}_3\delta\dot{u}_3\right)\mathrm{d}V = \frac{1}{2}\int_A \big[I_0\left(\dot{u}_1^0\delta\dot{u}_1^0 + \dot{u}_2^0\delta\dot{u}_2^0 + \dot{u}_3^0\delta\dot{u}_3^0\right)\\ + I_1\left(\dot{u}_1^0\delta\dot{u}_{3,1}^0 + \dot{u}_{3,1}^0\delta\dot{u}_1^0 + \dot{u}_2^0\delta\dot{u}_{3,2}^0 + \dot{u}_{3,2}^0\delta\dot{u}_2^0\right)\\ + J_2\left(\dot{u}_{3,1}^0\delta\dot{\varphi}_1 + \dot{\varphi}_1\delta\dot{u}_{3,1}^0 + \dot{u}_{3,2}^0\delta\dot{\varphi}_2 + \dot{\varphi}_2\delta\dot{u}_{3,2}^0\right) + K_2\left(\dot{\varphi}_1\delta\dot{\varphi}_1 + \dot{\varphi}_2\delta\dot{\varphi}_2\right)\\ + J_1\left(\dot{u}_1^0\delta\dot{\varphi}_1 + \dot{\varphi}_1\delta\dot{u}_1^0 + \dot{u}_2^0\delta\dot{\varphi}_2 + \dot{\varphi}_2\delta\dot{u}_2^0\right) + I_2\left(\dot{u}_{3,1}^0\delta\dot{u}_{3,1}^0 + \dot{u}_{3,2}^0\delta\dot{u}_{3,2}^0\right)\big]\mathrm{d}A,\end{aligned} \tag{20}$$

where $I_0, I_1, I_2, J_1, J_2, K_2$ are mass inertias of the FGP microplates which are defined as follows

$$\left(I_0, I_1, I_2, J_1, J_2, K_2\right) = \int_{-h/2}^{h/2}\left(1, \Phi_1, \Phi_1^2, \Phi_2, \Phi_1\Phi_2, \Phi_2^2\right)\rho\mathrm{d}x_3. \tag{21}$$

3. RITZ-BASED SOLUTIONS

Based on the Ritz method, the membrane and transverse displacements, rotations $\left(u_1^0, u_2^0, u_3^0, \varphi_1, \varphi_2\right)$ of the FGP microplates can be expressed in terms of the series of approximation functions and associated values of series as follows

$$u_1^0\left(x_1, x_2\right) = \sum_{i=1}^{n_1}\sum_{j=1}^{n_2} u_{1ij}R_{i,1}\left(x_1\right)P_j\left(x_2\right), \quad u_2^0\left(x_1, x_2\right) = \sum_{i=1}^{n_1}\sum_{j=1}^{n_2} u_{2ij}R_i\left(x_1\right)P_{j,2}\left(x_2\right), \tag{22a}$$

$$u_3^0\left(x_1, x_2\right) = \sum_{i=1}^{n_1}\sum_{j=1}^{n_2} u_{3ij}R_i\left(x_1\right)P_j\left(x_2\right), \quad \varphi_1\left(x_1, x_2\right) = \sum_{i=1}^{n_1}\sum_{j=1}^{n_2} x_{ij}R_{i,1}\left(x_1\right)P_j\left(x_2\right), \tag{22b}$$

$$\varphi_2\left(x_1, x_2\right) = \sum_{i=1}^{n_1}\sum_{j=1}^{n_2} y_{ij}R_i\left(x_1\right)P_{j,2}\left(x_2\right), \tag{22c}$$

where $u_{1ij}, u_{2ij}, u_{3ij}, x_{ij}, y_{ij}$ are variables to be determined; $R_i\left(x_1\right), P_j\left(x_2\right)$ are the shape functions in x_1-, x_2-direction, respectively. As a result, five unknowns of the plate only depend on two shape functions. It should be noted that the accuracy, convergence rates and numerical instabilities of the Ritz solution depends on the selection of the shape functions, which was discussed in details in [27–32]. The functions $R_i\left(x_1\right)$ and $P_j\left(x_2\right)$ given in Table 1 are constructed to satisfy the boundary conditions (BCs) at the plate edges in which two following kinematic typical BCs are considered

- Simply supported (S): $u_2^0 = u_3^0 = \varphi_2 = 0$ at $x_1 = 0, a$ and $u_1^0 = u_3^0 = \varphi_1 = 0$ at $x_2 = 0, b$.
- Clamped (C): $u_1^0 = u_2^0 = u_3^0 = \varphi_1 = \varphi_2 = 0$ at $x_1 = 0, a$ and $x_2 = 0, b$.

Table 1. Approximation functions of series solutions with different boundary conditions [28]

Boundary conditions	Approximation functions	
	$R_j(x_1)$	$P_j(x_2)$
SSSS	$x_1(a-x_1)e^{-\frac{jx_1}{a}}$	$x_2(b-x_2)e^{-\frac{jx_2}{a}}$
CCCC	$x_1^2(a-x_1)^2e^{-\frac{jx_1}{a}}$	$x_2^2(b-x_2)^2e^{-\frac{jx_2}{b}}$
SCSC	$x_1(a-x_1)^2e^{-\frac{jx_1}{a}}$	$x_2(b-x_2)^2e^{-\frac{jx_2}{b}}$

The combination of S and C on the edges leads to the different BCs, in which SSSS, SCSC, CCCC in Table 1 are chosen to investigate in this paper. Furthermore, in order to derive characteristic equations of motion of the FGP microplates, substituting the approximations in Eq. (22) into Eqs. (20), (19), (17) and then the subsequent results into Eq. (16) lead to

$$\mathbf{K}\mathbf{d}+\mathbf{M}\ddot{\mathbf{d}}=\mathbf{F}, \tag{23}$$

where $\mathbf{d}=\begin{bmatrix}\mathbf{u}_1 & \mathbf{u}_2 & \mathbf{u}_3 & \mathbf{x} & \mathbf{y}\end{bmatrix}^T$ is the displacement vector to be determined; $\mathbf{K}=\mathbf{K}^{\varepsilon}+\mathbf{K}^{\chi}+\mathbf{K}^{\tilde{\xi}}+\mathbf{K}^{\eta}$ is the stiffness matrix which is composed of those of the strains $\mathbf{K}^{\varepsilon}$, symmetric rotation gradients $\mathbf{K}^{\chi}$, dilatation gradient $\mathbf{K}^{\tilde{\xi}}$, and deviation stretch gradient $\mathbf{K}^{\eta}$; $\mathbf{M}$ is the mass matrix, and $\mathbf{F}$ is the force vector. These components are given more details as follows

$$\mathbf{K}^{\zeta}=\begin{bmatrix}\mathbf{K}^{\zeta 11} & \mathbf{K}^{\zeta 12} & \mathbf{K}^{\zeta 13} & \mathbf{K}^{\zeta 14} & \mathbf{K}^{\zeta 15}\\ {}^{T}\mathbf{K}^{\zeta 12} & \mathbf{K}^{\zeta 22} & \mathbf{K}^{\zeta 23} & \mathbf{K}^{\zeta 24} & \mathbf{K}^{\zeta 25}\\ {}^{T}\mathbf{K}^{\zeta 13} & {}^{T}\mathbf{K}^{\zeta 23} & \mathbf{K}^{\zeta 33} & \mathbf{K}^{\zeta 34} & \mathbf{K}^{\zeta 35}\\ {}^{T}\mathbf{K}^{\zeta 14} & {}^{T}\mathbf{K}^{\zeta 24} & {}^{T}\mathbf{K}^{\zeta 34} & \mathbf{K}^{\zeta 44} & \mathbf{K}^{\zeta 45}\\ {}^{T}\mathbf{K}^{\zeta 15} & {}^{T}\mathbf{K}^{\zeta 25} & {}^{T}\mathbf{K}^{\zeta 35} & {}^{T}\mathbf{K}^{\zeta 45} & \mathbf{K}^{\zeta 55}\end{bmatrix} \text{ with } \zeta=\{\varepsilon,\tilde{\xi},\chi,\eta\}, \tag{24a}$$

$$\mathbf{M}=\begin{bmatrix}\mathbf{M}^{11} & 0 & \mathbf{M}^{13} & \mathbf{M}^{14} & 0\\ 0 & \mathbf{M}^{22} & \mathbf{M}^{23} & 0 & \mathbf{M}^{25}\\ {}^{T}\mathbf{M}^{13} & {}^{T}\mathbf{M}^{23} & \mathbf{M}^{33} & \mathbf{M}^{34} & \mathbf{M}^{35}\\ {}^{T}\mathbf{M}^{14} & 0 & {}^{T}\mathbf{M}^{34} & \mathbf{M}^{44} & \mathbf{M}^{45}\\ 0 & {}^{T}\mathbf{M}^{25} & {}^{T}\mathbf{M}^{35} & {}^{T}\mathbf{M}^{45} & \mathbf{M}^{55}\end{bmatrix}, \tag{24b}$$

$$\mathbf{F}=\begin{bmatrix}\mathbf{0} & \mathbf{0} & \mathbf{f} & \mathbf{0} & \mathbf{0}\end{bmatrix}^T, \tag{24c}$$

where the components of mass matrix $\mathbf{M}$, stiffness matrix $\mathbf{K}^{\varepsilon}$ and $\mathbf{K}^{\chi}$ can be seen in [29]. The components of stiffness matrix $\mathbf{K}^{\tilde{\xi}}$, $\mathbf{K}^{\eta}$ and load vector $\mathbf{F}$ are give in Appendix C.

It is worth to notice that for static analysis, the static responses of the FGP microplates can be obtained from Eq. (23) by ignoring inertia terms. For free vibration analysis, by denoting $\mathbf{d}(t)=\mathbf{d}e^{i\omega t}$ where ω is the natural frequency of the FGP microplates and $i^2=-1$ is imaginary unit, the natural frequencies can be derived from the following characteristic equation: $\left(\mathbf{K}-\omega^2\mathbf{M}\right)\mathbf{d}=\mathbf{0}$.

4. NUMERICAL RESULTS

In this section, numerical examples are carried out to investigate static and free vibration behaviours of FGP microplates with different BCs in which the Reddy's shear function [33] $f(x_3) = x_3 - 4x_3^3/3h^2$ is employed. They are assumed to be made of a ceramic-metal mixture whose material properties are given as follows: Al_2O_3 ($E_c = 380$ GPa, $\rho_c = 3800\ \mathrm{kg/m^3}, v_c = 0.3$), Al ($E_m = 70$ GPa, $\rho_m = 2702\ \mathrm{kg/m^3}, v_m = 0.3$). For simplification purpose, all three MLSPs are assumed to have identical values $l_1 = l_2 = l_3 = l$ and they should be determined by experimental works. For convenience, the following normalized parameters are used in the computations

$$\overline{w} = \frac{10E_c h^3}{qa^4} u_3\left(\frac{a}{2}, \frac{b}{2}\right), \quad \overline{\omega} = \frac{\omega a^2}{h}\sqrt{\frac{\rho_c}{E_c}}. \tag{25}$$

Table 2. Convergence study of series solution of Al/Al_2O_3 FGP microplates with different boundary conditions ($a/h = 10, p = 5, \beta = 0.1, h/l = \infty$)

Solution	Number of series $n = n_1 = n_2$						
	2	4	6	8	10	12	14
Normalized center deflection							
SSSS	1.1801	1.2159	1.2191	1.2182	1.2184	1.2183	1.2184
SCSC	0.7287	0.7136	0.7022	0.7016	0.7015	0.7016	0.7016
CCCC	0.4870	0.4863	0.4824	0.4828	0.4822	0.4827	0.4826
Normalized fundamental frequency							
SSSS	3.4897	3.4630	3.4560	3.4567	3.4551	3.4574	3.4573
SCSC	5.1482	4.6407	4.6179	4.6148	4.6224	4.7171	4.7172
CCCC	6.0479	5.9494	5.9035	5.8888	5.8843	5.8837	5.8838

In order to verify the convergence of present solutions, Table 2 shows the transverse center displacement and fundamental frequency of Al/Al_2O_3 FGP square microplates under a sinusoidal distributed load and with $a/h = 10, p = 5, \beta = 0.1, h/l = \infty$. The results are calculated with three types of boundary conditions (SSSS, SCSC, CCCC) and the same number of series in x_1- and x_2-direction ($n_1 = n_2 = n$). It is observed from Table 2 that the solutions converge very quickly, and the number of series $n = 12$ can be considered as a convergence point of the static and dynamic responses of the FGP microplates. Thus, this number of series will be used for numerical computations.

4.1. Static analysis

In order to verify the accuracy of the present FGP microplate model in predicting static behaviours, the first example is performed on the simply supported FG square microplates subjected to sinusoidally distributed loads without porosity effect ($\beta = 0$). Various values of the power-law index p, length-to-thickness ratio a/h, and thickness-to-MLSP ratio h/l are considered for static responses of Al/Al_2O_3 FG microplates. The

obtained results are reported in Tables 3 and 4, and compared with those derived from Thai et al. [22], Thai et al. [25] using the MST, isogeometric approach and HSDT, Zhang et al. [34] using the MST, Navier method and HSDT. It can be seen that there are good agreements between the models for different BCs, material distribution and size effects, which shows the accuracy of present approach for static behaviours.

Table 3. Normalized transverse center displacements of FGP microplates under sinusoidal load ($\beta = 0$, SSSS)

a/h	p	Theory	h/l					
			0	20	10	5	2	1
5	0.5	Present	0.5177	0.4957	0.4411	0.3065	0.1011	0.0292
		MST [22]	0.5176	0.4965	0.4426	0.3098	0.1018	0.0303
		RPT [34]	0.5198	0.4983	0.4435	0.3086	0.0997	0.0293
		IGA [25]	0.5177	0.4975	0.4457	0.3153	0.1045	0.0310
	1	Present	0.6688	0.6387	0.5625	0.3860	0.1226	0.0353
		MST [22]	0.6688	0.6399	0.5670	0.3908	0.1252	0.0369
		RPT [34]	0.6688	0.6396	0.5658	0.3879	0.1223	0.0357
		IGA [25]	0.6688	0.6412	0.5709	0.3977	0.1286	0.0378
	2	Present	0.8672	0.8261	0.7256	0.5021	0.1521	0.0442
		MST [22]	0.8671	0.8292	0.7332	0.5021	0.1580	0.0460
		RPT [34]	0.8671	0.8286	0.7313	0.4980	0.1544	0.0447
		IGA [25]	0.8671	0.8307	0.7379	0.5107	0.1627	0.0475
	4	Present	1.0411	0.9899	0.8681	0.6024	0.1898	0.0552
		MST [22]	1.0409	0.9977	0.8875	0.6159	0.1964	0.0573
		RPT [34]	1.0408	0.9967	0.8843	0.6095	0.1921	0.0558
		IGA [25]	1.0409	0.9994	0.8927	0.6263	0.2034	0.0597
	10	Present	1.2279	1.1681	1.0282	0.7443	0.2455	0.0728
		MST [22]	1.2276	1.1811	1.0609	0.7548	0.2510	0.0743
		RPT [34]	1.2269	1.1790	1.0557	0.7455	0.2454	0.0724
		IGA [25]	1.2276	1.1829	1.0668	0.7678	0.2614	0.0781
10	0.5	Present	0.4538	0.4361	0.3884	0.2747	0.0895	0.0263
		MST [22]	0.4537	0.4355	0.3887	0.2723	0.0884	0.0260
	1	Present	0.5890	0.5646	0.5003	0.3479	0.1106	0.0322
		MST [22]	0.5890	0.5640	0.5004	0.3453	0.1095	0.0320
	2	Present	0.7572	0.7258	0.6426	0.4463	0.1418	0.0412
		MST [22]	0.7573	0.7253	0.6439	0.4446	0.1407	0.0409
	4	Present	0.8814	0.8475	0.7588	0.5404	0.1797	0.0531
		MST [22]	0.8815	0.8480	0.7614	0.5405	0.1784	0.0526
	10	Present	1.0086	0.9739	0.8808	0.6497	0.2325	0.0707
		MST [22]	1.0087	0.9755	0.8879	0.6535	0.2298	0.0694

Table 4. Normalized transverse center displacements of FGP microplates under sinusoidal load with $a/h = 10$

BCs	p	Theory	h/l					
			0	20	10	5	2	1
CCCC	0.5	Present	0.1755	0.1677	0.1488	0.1032	0.0331	0.0099
		MST [22]	0.1747	0.1675	0.1492	0.1042	0.0340	0.0100
		IGA [25]	0.1773	-	0.1521	0.1068	0.0349	0.0103
	1	Present	0.2271	0.2165	0.1909	0.1306	0.0412	0.0121
		MST [22]	0.2261	0.2163	0.1951	0.1349	0.0419	0.0123
		IGA [25]	0.2295	-	0.1915	0.1318	0.0430	0.0126
	2	Present	0.2936	0.2794	0.2456	0.1673	0.0529	0.0158
		MST [22]	0.2922	0.2794	0.2472	0.1694	0.0532	0.0155
		IGA [25]	0.2967	-	0.2517	0.1733	0.0547	0.0159
	5	Present	0.3631	0.3452	0.3047	0.2124	0.0706	0.0211
		MST [22]	0.3609	0.3466	0.3100	0.2182	0.0712	0.0209
		IGA [25]	0.3676	-	0.3161	0.2233	0.0734	0.0216
	10	Present	0.4068	0.3873	0.3436	0.2437	0.0838	0.0252
		MST [22]	0.4041	0.3893	0.3582	0.2523	0.0854	0.0254
		IGA [25]	0.4121	-	0.3510	0.2584	0.0884	0.0265
SCSC	0.5	Present	0.2585	0.2477	0.2198	0.1514	0.0477	0.0139
		IGA [25]	0.2472	-	0.2122	0.1492	0.0488	0.0144
	1	Present	0.3349	0.3200	0.2823	0.1917	0.0591	0.0171
		IGA [25]	0.3201	-	0.2724	0.1886	0.0602	0.0176
	2	Present	0.4318	0.4126	0.3643	0.2480	0.0769	0.0221
		IGA [25]	0.4133	-	0.3513	0.2425	0.0768	0.0223
	5	Present	0.5256	0.5055	0.4540	0.3218	0.1059	0.0311
		IGA [25]	0.5086	-	0.4389	0.3118	0.1035	0.0306
	10	Present	0.5849	0.5646	0.5118	0.3720	0.1280	0.0382
		IGA [25]	0.5685	-	0.4961	0.3604	0.1246	0.0375

Moreover, in order to investigate effects of porosity β, material parameter p, side-to-thickness ratio a/h, size effects h/l and boundary conditions on the static responses of FGP microplates, Table 5 presents the normalized center transverse displacements with various configurations. The variations of center deflections with respect to a/h and h/l are also plotted in Fig. 1. It can be seen that the transverse displacements increase with increase of the p and h/l. The graph in Fig. 1(b) reveals that the deflections vary gradually for $h/l \leq 10$ and from $h/l = 25$ the curves become flatter and the results tend to be closed to those obtained from the classical theory $(h/l = \infty)$, which explains that the size effects on deflections of FGP microplates are not significant from $h/l > 25$.

Table 5. Normalized transverse center displacements of FGP square microplates under sinusoidal load with different boundary conditions

BCs	a/h	β	p	h/l				
				∞	10	5	2	1
SSSS	10	0.1	0.5	0.5111	0.4342	0.3025	0.0962	0.0280
			1	0.6947	0.5831	0.3964	0.1218	0.0351
			2	0.9578	0.7987	0.5365	0.1622	0.0464
			5	1.2183	1.0372	0.7244	0.2345	0.0687
			10	1.3565	1.1739	0.8523	0.2968	0.0891
		0.2	0.5	0.5822	0.4903	0.3356	0.1043	0.0301
			1	0.8456	0.6983	0.4610	0.1361	0.0387
			2	1.3214	1.0690	0.6800	0.1909	0.0536
			5	1.9318	1.5884	1.0391	0.3052	0.0870
			10	2.1828	1.8440	1.2843	0.4187	0.1231
SCSC	10	0.1	0.5	0.2906	0.2449	0.1662	0.0512	0.0149
			1	0.3939	0.3278	0.2177	0.0653	0.0187
			2	0.5436	0.4503	0.2971	0.0882	0.0249
			5	0.7016	0.5956	0.4110	0.1301	0.0373
			10	0.7870	0.6844	0.4904	0.1641	0.0483
		0.2	0.5	0.3305	0.2758	0.1841	0.0552	0.0159
			1	0.4781	0.3909	0.2525	0.0729	0.0206
			2	0.7462	0.5979	0.3749	0.1033	0.0288
			5	1.1042	0.9064	0.5905	0.1675	0.0476
			10	1.2676	1.0785	0.7459	0.2348	0.0674
CCCC	10	0.1	0.5	0.1969	0.1640	0.1100	0.0335	0.0101
			1	0.2663	0.2191	0.1439	0.0426	0.0128
			2	0.3682	0.3012	0.1962	0.0573	0.0164
			5	0.4827	0.4036	0.2735	0.0844	0.0244
			10	0.5480	0.4671	0.3281	0.1070	0.0315
		0.2	0.5	0.2233	0.1842	0.1216	0.0362	0.0104
			1	0.3219	0.2603	0.1664	0.0475	0.0135
			2	0.5018	0.3975	0.2462	0.0676	0.0210
			5	0.7550	0.6090	0.3888	0.1106	0.0313
			10	0.8832	0.7357	0.4969	0.1526	0.0440

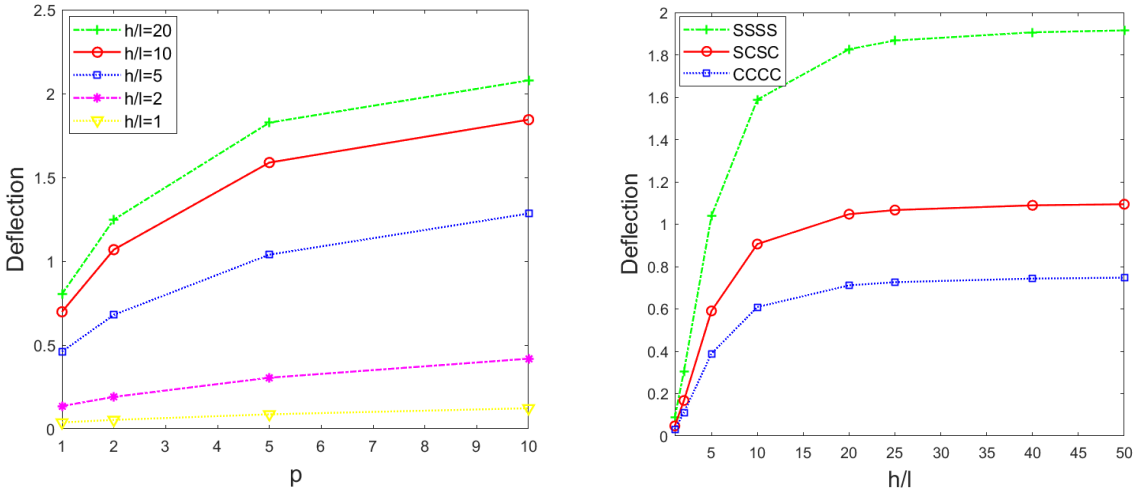

(a) SSSS (b) $p = 5$

Fig. 1. Variation of normalized center deflection with respect the power index p and thickness-to-length scale h/l of FGP microplates ($\beta = 0.2, a/h = 10$)

4.2. Free vibration analysis

In order to study the accuracy of present solutions in predicting vibration responses, Tables 6 and 7 provide the fundamental frequencies of Al/Al_2O_3 FGP microplates without porosity effects ($\beta = 0$) in which the solutions are computed for various configurations. The obtained results are compared with those derived from Thai et al. [22] and Thai et al. [25] based on the MST, IGA and HSDT, Zhang et al. [34] based on the MST and Navier procedure and a refined HSDT. It can be seen that there is no discrepancy between models. The fundamental frequencies decrease with the increase of p as expected.

Table 6. Normalized fundamental frequencies $\overline{\omega} = \omega h\sqrt{\rho_c/E_c}$ of Al/Al_2O_3 FGP square microplates ($\beta = 0$, $a/h = 10$, SSSS)

p	Theory	h/l				
		∞	10	5	2	1
0	Present	0.0577	0.0615	0.0726	0.1250	0.2283
	MST [22]	0.0577	0.0619	0.0729	0.1254	0.2297
	RPT [34]	0.0577	0.0619	0.0730	0.1258	0.2309
	IGA [25]	0.0577	0.0617	0.0725	0.1240	0.2268
0.5	Present	0.0490	0.0529	0.0626	0.1099	0.2035
	MST [22]	0.0490	0.0529	0.0633	0.1110	0.2047
	RPT [34]	0.0489	0.0529	0.0632	0.1113	0.2057
	IGA [25]	0.0490	0.0528	0.0629	0.1098	0.2023

p	Theory	h/l				
		∞	10	5	2	1
1	Present	0.0441	0.0475	0.0574	0.1014	0.1884
	MST [22]	0.0442	0.0479	0.0577	0.1024	0.1896
	RPT [34]	0.0442	0.0480	0.0578	0.1028	0.1907
	IGA [25]	0.0442	0.0478	0.0573	0.1013	0.1873
2	Present	0.0401	0.0431	0.0520	0.0926	0.1722
	MST [22]	0.0401	0.0435	0.0523	0.0930	0.1722
	RPT [34]	0.0401	0.0435	0.0524	0.0933	0.1731
	IGA [25]	0.0401	0.0434	0.0520	0.0918	0.1698
	MST [22]	0.0377	0.0404	0.0477	0.0822	0.1508
	RPT [34]	0.0377	0.0405	0.0478	0.0825	0.1514
	IGA [25]	0.0377	0.0403	0.0474	0.0810	0.1482
10	Present	0.0364	0.0388	0.0452	0.0757	0.1360
	MST [22]	0.0363	0.0387	0.0451	0.0761	0.1384
	RPT [34]	0.0364	0.0388	0.0453	0.0764	0.1390
	IGA [25]	0.0364	0.0387	0.0449	0.0750	0.1359

Table 7. Normalized fundamental frequencies of Al/Al_2O_3 FGP square microplates ($\beta = 0, a/h = 10$, CCCC and SCSC)

BCs	p	Theory	h/l					
			∞	20	10	5	2	1
CCCC	0.5	Present	8.4735	8.6614	9.1920	11.0307	18.9020	35.1640
		IGA [25]	8.4405	-	9.1227	10.8954	19.0701	35.1215
	1	Present	7.6782	7.8132	8.3908	10.0530	17.6636	32.3192
		IGA [25]	7.6251	-	8.2766	9.9597	17.6422	32.6292
	2	Present	6.9176	7.1106	7.5746	9.0783	15.9206	28.8231
		IGA [25]	6.8944	-	7.4923	9.0367	16.0977	29.8609
	5	Present	6.4231	6.5519	6.9710	8.3300	13.9971	25.9460
		IGA [25]	6.3722	-	6.8823	8.2026	14.3324	26.4157
	10	Present	6.1199	6.2784	6.6505	7.8617	13.0441	23.9971
		IGA [25]	6.1039	-	6.5602	7.7407	13.2706	24.2754
SCSC	0.5	Present	6.7197	6.8676	7.2931	8.7900	15.6599	29.0008
		IGA [25]	6.9031	-	7.4556	8.8961	15.5600	28.6567
	1	Present	6.0650	6.2057	6.6094	8.0210	14.4368	26.8247
		IGA [25]	6.2329	-	6.7605	8.1283	14.3915	26.6161
	2	Present	5.4955	5.6222	5.9858	7.2578	13.0467	24.2396
		IGA [25]	5.6405	-	6.1230	7.3744	13.1146	24.3082
	5	Present	5.1361	5.2381	5.5323	6.5758	11.4606	21.0871
		IGA [25]	5.2361	-	5.6429	6.7021	11.6480	21.4179
	10	Present	4.9452	5.0338	5.2903	6.2080	10.5865	19.3316
		IGA [25]	5.0254	-	5.3868	6.3288	10.7777	19.6645

Table 8. Normalized fundamental frequencies of Al/Al_2O_3 FGP square microplates

BCs	a/h	β	p	h/l				
				∞	10	5	2	1
SSSS	10	0.1	0.5	4.8469	5.2465	6.2753	11.1444	20.5884
			1	4.2815	4.6668	5.6497	10.2161	19.0334
			2	3.7640	4.1238	4.9947	9.1029	16.9999
			5	3.4574	3.6783	4.4653	7.8075	14.4907
			10	3.3327	3.5350	4.1840	7.0993	12.8651
		0.2	0.5	4.7972	5.2009	6.1126	11.1001	20.1158
			1	4.1121	4.5268	5.5541	10.0543	19.0057
			2	3.4064	3.7713	4.7471	8.9419	16.8823
			5	2.9323	3.2158	3.9832	7.3159	13.7288
			10	2.8148	3.0352	3.6550	6.4101	11.7388
SCSC	10	0.1	0.5	6.6598	7.2591	8.7147	15.3799	28.4118
			1	5.8920	6.4631	7.9308	14.1016	26.1753
			2	5.1741	5.6891	7.0084	12.5850	23.7134
			5	4.7171	5.1198	6.1693	10.9865	20.3606
			10	4.5305	4.8659	5.7523	9.9342	18.2235
		0.2	0.5	6.5990	7.1277	8.5988	15.1299	28.1844
			1	5.6709	6.2750	7.7094	14.0535	26.0222
			2	4.6990	5.2527	6.6405	12.5620	23.6336
			5	4.0124	4.4345	5.5079	10.2385	19.2228
			10	3.8229	4.1489	4.9977	8.8931	16.4769
CCCC	10	0.1	0.5	8.3865	9.1064	11.0009	18.7157	35.0700
			1	7.4713	8.1995	9.9376	17.5254	32.1417
			2	6.5451	7.2033	8.8372	15.7657	28.6778
			5	5.8837	6.1920	7.8150	13.3725	23.7300
			10	5.6264	6.1831	7.3008	12.0451	21.4739
		0.2	0.5	8.3202	9.1037	11.0001	18.6797	34.9638
			1	7.1684	7.9717	9.7343	17.3071	32.1207
			2	5.9501	6.6362	8.3403	15.2109	28.4556
			5	5.0257	5.6144	6.9379	11.9968	20.3562
			10	4.7414	5.2673	6.3223	10.5215	19.6228

The effect of p on the natural frequencies of Al/Al_2O_3 FGP microplates is also plotted in Fig. 2(a) for $h/l = 1, 2, 5, 10, 20, a/h = 10$ and $\beta = 0.2$. There exist large deviations of these curves, which indicate significant size effects. Moreover, the variations of fundamental frequencies with respect to h/l are displayed in Fig. 2(b). It is observed that the results decrease with the increase of h/l up to $h/l = 10$ and then the curves become flatter which indicates the size effects can be neglected.

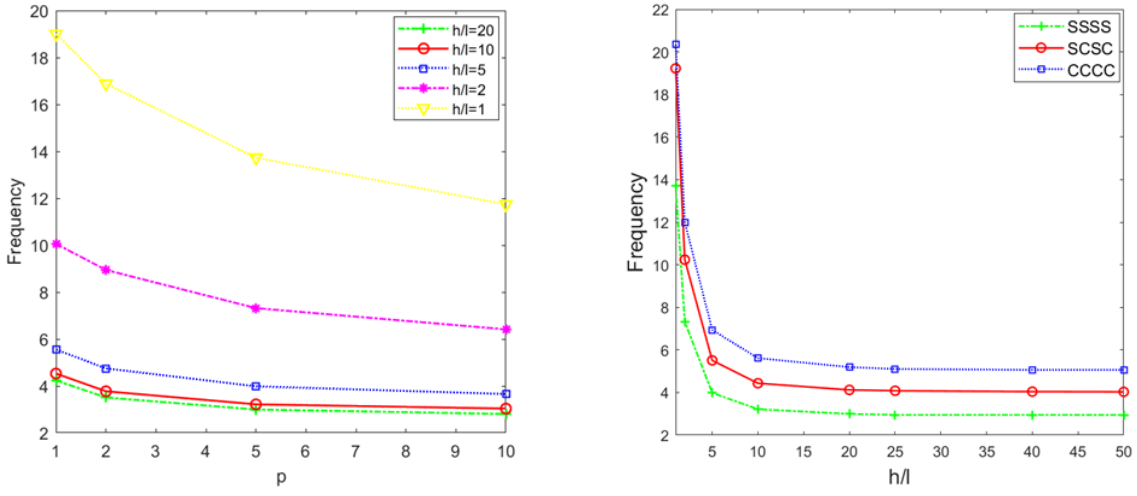

(a) SSSS (b) $p = 5$

Fig. 2. Variation of normalized fundamental frequencies with respect the power index p and thickness-to-MLSP ratio h/l $(a/h = 10, \beta = 0.2)$

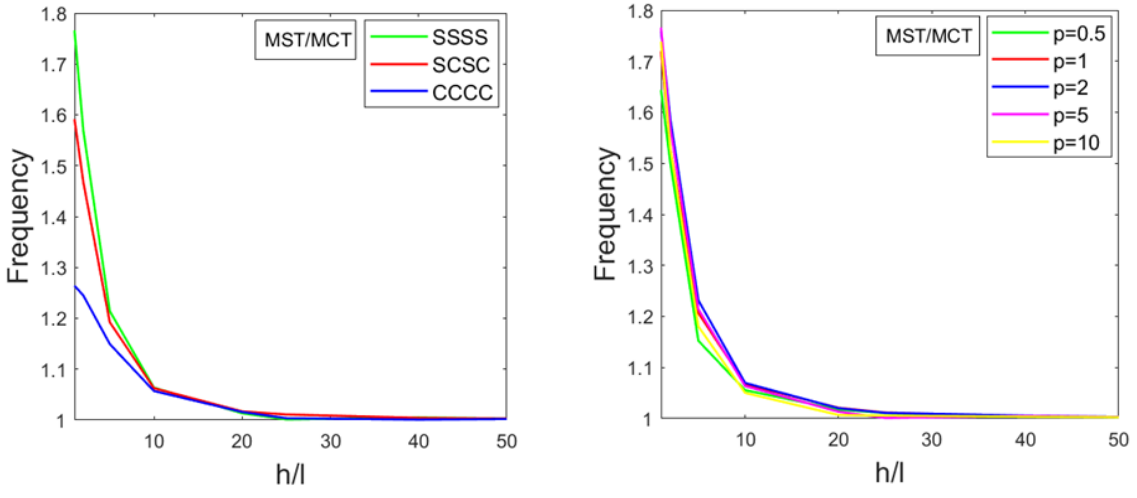

(a) $p = 5$ (b) SSSS

Fig. 3. Size effect of the MCT and MST for the normalised fundamental frequencies with respect to the length scale-to-thickness ratio h/l $(\beta = 0.2, p = 5, a/h = 10)$

In order to study further the size effects of vibration problems, Fig. 3 illustrates the ratio of fundamental frequencies computed from the MST over the MCT, which is expressed with respect to $h/l, p = 5, \beta = 0.2, a/h = 10$ and different boundary conditions. It can be observed that the MST with three MLSPs produces frequencies larger than the

MCT with one MLSP, especially when the Static and vibration analysis of functionally graded microplate with porosities based on higher-order shear deformation and modified strain gradient theory microplate thickness is close to the MLSP. It emphasizes the importance of the consideration of three components e.g. the dilatation, deviatoric stretch and symmetric part of rotation gradient tensor in the MST rather than only the symmetric part of rotation gradient tensor in the MCT when dealing with microplates. As expected, by increasing the size scale, the difference between the theories is decreased.

5. CONCLUSIONS

A unified higher-order shear deformation theory and modified strain gradient theory have been developed in this paper for static and free vibration analyses of functionally graded porous microplates. The equations of motion are derived from Hamilton's principle and series-type approximation with exponential shape functions. Numerical examples are presented to investigate effects of side-tothickness ratio, thickness-to-material length scale parameter ratio and boundary conditions on the deflections and natural frequencies of FGP microplates. The obtained results show that the size effects lead to an increase in the stiffness of the FGP microplates, consequently it decreases their transverse displacements and increases their natural frequencies. Significant differences of the present theory and modified couple stress theory are observed when the microplate thickness and MLSP is the same dimension, it shows that the dilatation and deviatoric stretch should be accounted for computations of microplates. The present theory is found to be accurate and efficient in predicting static and dynamic behaviours of FGP microplates.

DECLARATION OF COMPETING INTEREST

The authors declare that they have no known competing financial interests or personal relationships that could have appeared to influence the work reported in this paper.

FUNDING

This research received no specific grant from any funding agency in the public, commercial, or not-for-profit sectors.

REFERENCES

[1] N. Jalili and K. Laxminarayana. A review of atomic force microscopy imaging systems: application to molecular metrology and biological sciences. *Mechatronics*, **14**, (2004), pp. 907–945. https://doi.org/10.1016/j.mechatronics.2004.04.005.

[2] D. Ozevin. Micro-electro-mechanical-systems (MEMS) for assessing and monitoring civil infrastructures. In *Sensor Technologies for Civil Infrastructures*, pp. 265–302e. Elsevier, (2014). https://doi.org/10.1533/9780857099136.265.

[3] P. A. Demirhan and V. Taskin. Bending and free vibration analysis of Levy-type porous functionally graded plate using state space approach. *Composites Part B: Engineering*, **160**, (2019), pp. 661–676. https://doi.org/10.1016/j.compositesb.2018.12.020.

[4] D. Chen, J. Yang, and S. Kitipornchai. Buckling and bending analyses of a novel functionally graded porous plate using Chebyshev-Ritz method. *Archives of Civil and Mechanical Engineering*, **19**, (2019), pp. 157–170. https://doi.org/10.1016/j.acme.2018.09.004.

[5] J. Zhao, K. Choe, F. Xie, A. Wang, C. Shuai, and Q. Wang. Three-dimensional exact solution for vibration analysis of thick functionally graded porous (FGP) rectangular plates with arbitrary boundary conditions. *Composites Part B: Engineering*, **155**, (2018), pp. 369–381. https://doi.org/10.1016/j.compositesb.2018.09.001.

[6] K. Li, D. Wu, X. Chen, J. Cheng, Z. Liu, W. Gao, and M. Liu. Isogeometric Analysis of functionally graded porous plates reinforced by graphene platelets. *Composite Structures*, **204**, (2018), pp. 114–130. https://doi.org/10.1016/j.compstruct.2018.07.059.

[7] M. Dhuria, N. Grover, and K. Goyal. Influence of porosity distribution on static and buckling responses of porous functionally graded plates. *Structures*, **34**, (2021), pp. 1458–1474. https://doi.org/10.1016/j.istruc.2021.08.050.

[8] N. V. Nguyen, H. Nguyen-Xuan, D. Lee, and J. Lee. A novel computational approach to functionally graded porous plates with graphene platelets reinforcement. *Thin-Walled Structures*, **150**, (2020). https://doi.org/10.1016/j.tws.2020.106684.

[9] S. Merdaci and H. Belghoul. High-order shear theory for static analysis of functionally graded plates with porosities. *Comptes Rendus Mécanique*, **347**, (2019), pp. 207–217. https://doi.org/10.1016/j.crme.2019.01.001.

[10] A. M. Zenkour and M. H. Aljadani. Quasi-3D refined theory for functionally graded porous plates: Vibration analysis. *Physical Mesomechanics*, **24**, (2021), pp. 243–256. https://doi.org/10.1134/s1029959921030036.

[11] V. T. Long and H. V. Tung. Thermal nonlinear buckling of shear deformable functionally graded cylindrical shells with porosities. *AIAA Journal*, **59**, (2021), pp. 2233–2241. https://doi.org/10.2514/1.j060026.

[12] V. T. Long and H. V. Tung. Thermomechanical nonlinear buckling of pressurized shear deformable FGM cylindrical shells including porosities and elastically restrained edges. *Journal of Aerospace Engineering*, **34**, (2021). https://doi.org/10.1061/(asce)as.1943-5525.0001252.

[13] V. T. Long and H. V. Tung. Thermo-torsional buckling and postbuckling of thin FGM cylindrical shells with porosities and tangentially restrained edges. *Mechanics Based Design of Structures and Machines*, (2022), pp. 1–20. https://doi.org/10.1080/15397734.2022.2084752.

[14] V. T. Long and H. V. Tung. Buckling and postbuckling of functionally graded porous material nearly cylindrical shells under external lateral pressure in thermal environments. *Ships and Offshore Structures*, (2022), pp. 1–9. https://doi.org/10.1080/17445302.2022.2100666.

[15] S. Kong. A review on the size-dependent models of micro-beam and micro-plate based on the modified couple stress theory. *Archives of Computational Methods in Engineering*, **29**, (2021), pp. 1–31. https://doi.org/10.1007/s11831-021-09567-w.

[16] F. Fan, Y. Xu, S. Sahmani, and B. Safaei. Modified couple stress-based geometrically nonlinear oscillations of porous functionally graded microplates using NURBS-based isogeometric approach. *Computer Methods in Applied Mechanics and Engineering*, **372**, (2020). https://doi.org/10.1016/j.cma.2020.113400.

[17] A. Farzam and B. Hassani. Size-dependent analysis of FG microplates with temperature-dependent material properties using modified strain gradient theory

and isogeometric approach. *Composites Part B: Engineering*, **161**, (2019), pp. 150–168. https://doi.org/10.1016/j.compositesb.2018.10.028.

[18] J. Kim, K. K. Żur, and J. N. Reddy. Bending, free vibration, and buckling of modified couples stress-based functionally graded porous micro-plates. *Composite Structures*, **209**, (2019), pp. 879–888. https://doi.org/10.1016/j.compstruct.2018.11.023.

[19] D. C. C. Lam, F. Yang, A. C. M. Chong, J. Wang, and P. Tong. Experiments and theory in strain gradient elasticity. *Journal of the Mechanics and Physics of Solids*, **51**, (2003), pp. 1477–1508. https://doi.org/10.1016/s0022-5096(03)00053-x.

[20] R. D. Mindlin. Second gradient of strain and surface-tension in linear elasticity. *International Journal of Solids and Structures*, **1**, (1965), pp. 417–438. https://doi.org/10.1016/0020-7683(65)90006-5.

[21] R. D. Mindlin and N. N. Eshel. On first strain-gradient theories in linear elasticity. *International Journal of Solids and Structures*, **4**, (1968), pp. 109–124. https://doi.org/10.1016/0020-7683(68)90036-x.

[22] C. H. Thai, A. J. M. Ferreira, and H. Nguyen-Xuan. Isogeometric analysis of size-dependent isotropic and sandwich functionally graded microplates based on modified strain gradient elasticity theory. *Composite Structures*, **192**, (2018), pp. 274–288. https://doi.org/10.1016/j.compstruct.2018.02.060.

[23] C. H. Thai, A. J. M. Ferreira, and P. Phung-Van. Size dependent free vibration analysis of multilayer functionally graded GPLRC microplates based on modified strain gradient theory. *Composites Part B: Engineering*, **169**, (2019), pp. 174–188. https://doi.org/10.1016/j.compositesb.2019.02.048.

[24] C. H. Thai, A. J. M. Ferreira, T. Rabczuk, and H. Nguyen-Xuan. Size-dependent analysis of FG-CNTRC microplates based on modified strain gradient elasticity theory. *European Journal of Mechanics - A/Solids*, **72**, (2018), pp. 521–538. https://doi.org/10.1016/j.euromechsol.2018.07.012.

[25] S. Thai, H.-T. Thai, T. P. Vo, and V. I. Patel. Size-dependant behaviour of functionally graded microplates based on the modified strain gradient elasticity theory and isogeometric analysis. *Computers & Structures*, **190**, (2017), pp. 219–241. https://doi.org/10.1016/j.compstruc.2017.05.014.

[26] C.-L. Thanh, L. V. Tran, T. Q. Bui, H. X. Nguyen, and M. Abdel-Wahab. Isogeometric analysis for size-dependent nonlinear thermal stability of porous FG microplates. *Composite Structures*, **221**, (2019). https://doi.org/10.1016/j.compstruct.2019.04.010.

[27] A. M. Zenkour and M. H. Aljadani. Porosity effect on thermal buckling behavior of actuated functionally graded piezoelectric nanoplates. *European Journal of Mechanics - A/Solids*, **78**, (2019). https://doi.org/10.1016/j.euromechsol.2019.103835.

[28] T.-K. Nguyen, H.-T. Thai, and T. P. Vo. A novel general higher-order shear deformation theory for static, vibration and thermal buckling analysis of the functionally graded plates. *Journal of Thermal Stresses*, (2021), pp. 1–21. https://doi.org/10.1080/01495739.2020.1869127.

[29] V.-T. Tran, T.-K. Nguyen, P. T. T. Nguyen, and T. P. Vo. Stochastic vibration and buckling analysis of functionally graded microplates with a unified higher-order shear deformation theory. *Thin-Walled Structures*, **177**, (2022). https://doi.org/10.1016/j.tws.2022.109473.

[30] M. Aydogdu. Buckling analysis of cross-ply laminated beams with general boundary conditions by Ritz method. *Composites Science and Technology*, **66**, (2006), pp. 1248–1255. https://doi.org/10.1016/j.compscitech.2005.10.029.

[31] M. Aydogdu. Vibration analysis of cross-ply laminated beams with general boundary conditions by Ritz method. *International Journal of Mechanical Sciences*, **47**, (2005), pp. 1740–1755. https://doi.org/10.1016/j.ijmecsci.2005.06.010.

[32] J. L. Mantari and F. G. Canales. Free vibration and buckling of laminated beams via hybrid Ritz solution for various penalized boundary conditions. *Composite Structures*, **152**, (2016), pp. 306–315. https://doi.org/10.1016/j.compstruct.2016.05.037.

[33] J. N. Reddy. *Mechanics of laminated composite plates and shells*. CRC Press, (2003). https://doi.org/10.1201/b12409.

[34] B. Zhang, Y. He, D. Liu, L. Shen, and J. Lei. An efficient size-dependent plate theory for bending, buckling and free vibration analyses of functionally graded microplates resting on elastic foundation. *Applied Mathematical Modelling*, **39**, (2015), pp. 3814–3845. https://doi.org/10.1016/j.apm.2014.12.001.

APPENDIX A

The non-zero components of dilatation gradients in Eq. (11) are defined by

$$\boldsymbol{\xi}^{(0)} = \begin{Bmatrix} \xi_1^{(0)} \\ \xi_2^{(0)} \\ \xi_3^{(0)} \end{Bmatrix} = \begin{Bmatrix} u^0_{1,11} + u^0_{2,12} \\ u^0_{1,12} + u^0_{2,22} \\ 0 \end{Bmatrix}, \quad \boldsymbol{\xi}^{(1)} = \begin{Bmatrix} \xi_1^{(1)} \\ \xi_2^{(1)} \\ \xi_3^{(1)} \end{Bmatrix} = \begin{Bmatrix} u^0_{3,111} + u^0_{3,122} \\ u^0_{3,112} + u^0_{3,222} \\ 0 \end{Bmatrix}, \tag{A.1a}$$

$$\boldsymbol{\xi}^{(2)} = \begin{Bmatrix} \xi_1^{(2)} \\ \xi_2^{(2)} \\ \xi_3^{(2)} \end{Bmatrix} = \begin{Bmatrix} \varphi_{1,11} + \varphi_{2,12} \\ \varphi_{1,12} + \varphi_{2,22} \\ 0 \end{Bmatrix}, \quad \boldsymbol{\xi}^{(3)} = \begin{Bmatrix} \xi_1^{(3)} \\ \xi_2^{(3)} \\ \xi_3^{(3)} \end{Bmatrix} = \begin{Bmatrix} 0 \\ 0 \\ u^0_{3,11} + u^0_{3,22} \end{Bmatrix}, \tag{A.1b}$$

$$\boldsymbol{\xi}^{(4)} = \begin{Bmatrix} \xi_1^{(4)} \\ \xi_2^{(4)} \\ \xi_3^{(4)} \end{Bmatrix} = \begin{Bmatrix} 0 \\ 0 \\ \varphi_{1,1} + \varphi_{2,2} \end{Bmatrix}.$$

The non-zero components of deviatoric stretch gradients η_{ijk} in Eq. (12) are given by

$$\eta_{111} = \varepsilon_{11,1} - \frac{1}{5}\left(\xi_1 + 2\varepsilon_{11,1} + \gamma_{12,2} + \gamma_{13,3}\right), \tag{A.2a}$$

$$\eta_{222} = \varepsilon_{22,2} - \frac{1}{5}\left(\xi_2 + 2\varepsilon_{22,2} + \gamma_{12,1} + \gamma_{23,3}\right),$$

$$\eta_{333} = -\frac{1}{5}\left(\xi_3 + \gamma_{13,1} + \gamma_{23,2}\right), \tag{A.2b}$$

$$\eta_{112} = \eta_{211} = \eta_{121} = \frac{1}{3}\left(\varepsilon_{11,2} + \gamma_{12,1}\right) - \frac{1}{15}\left(\xi_2 + \gamma_{12,1} + 2\varepsilon_{22,2} + \gamma_{23,3}\right),$$

$$\eta_{113} = \eta_{311} = \eta_{131} = \frac{1}{3}\left(\gamma_{13,1} + \varepsilon_{11,3}\right) - \frac{1}{15}\left(\xi_3 + \gamma_{13,1} + \gamma_{23,2}\right), \tag{A.2c}$$

$$\eta_{221} = \eta_{122} = \eta_{212} = \frac{1}{3}\left(\gamma_{12,2} + \varepsilon_{22,1}\right) - \frac{1}{15}\left(\xi_1 + 2\varepsilon_{11,1} + \gamma_{12,2} + \gamma_{13,3}\right), \tag{A.2d}$$

$$\eta_{223} = \eta_{322} = \eta_{232} = \frac{1}{3}\left(\gamma_{23,2} + \varepsilon_{22,3}\right) - \frac{1}{15}\left(\xi_3 + \gamma_{13,1} + \gamma_{23,2}\right), \tag{A.2e}$$

$$\eta_{331} = \eta_{133} = \eta_{313} = \frac{1}{3}\gamma_{13,3} - \frac{1}{15}\left(\xi_1 + 2\varepsilon_{11,1} + \gamma_{12,2} + \gamma_{13,3}\right), \tag{A.2f}$$

$$\eta_{332} = \eta_{233} = \eta_{323} = \frac{1}{3}\gamma_{23,3} - \frac{1}{15}\left(\xi_2 + \gamma_{12,1} + 2\varepsilon_{22,2} + \gamma_{23,3}\right), \tag{A.2g}$$

$$\eta_{123} = \eta_{231} = \eta_{312} = \eta_{132} = \eta_{321} = \eta_{213} = \frac{1}{6}\left(\gamma_{23,1} + \gamma_{13,2} + \gamma_{12,3}\right). \tag{A.2h}$$

These components can be expressed in terms of the displacements as follows

$$\boldsymbol{\eta}^{(0)} = \frac{1}{5}\begin{Bmatrix} 2u^0_{1,11} - 2u^0_{2,12} - u^0_{1,22} \\ 2u^0_{2,22} - 2u^0_{1,12} - u^0_{2,11} \\ 0 \\ -\left(3u^0_{1,11} + 2u^0_{2,12} + u^0_{1,22}\right) \\ -\left(3u^0_{2,22} + 2u^0_{1,12} + u^0_{2,11}\right) \\ 4u^0_{1,22} + 8u^0_{2,12} - 3u^0_{1,11} \\ 4u^0_{2,11} + 8u^0_{1,12} - 3u^0_{2,22} \\ 0 \\ 0 \\ 0 \end{Bmatrix}, \quad \boldsymbol{\eta}^{(1)} = \frac{1}{5}\begin{Bmatrix} 2u^0_{3,111} - 3u^0_{3,122} \\ 2u^0_{3,222} - 3u^0_{3,112} \\ 0 \\ -3\left(u^0_{3,111} + u^0_{3,122}\right) \\ -3\left(u^0_{3,112} + u^0_{3,222}\right) \\ 3\left(4u^0_{3,122} - u^0_{3,111}\right) \\ 3\left(4u^0_{3,112} - u^0_{3,222}\right) \\ 0 \\ 0 \\ 0 \end{Bmatrix}, \tag{A.3a}$$

$$\boldsymbol{\eta}^{(2)} = \frac{1}{5}\begin{Bmatrix} 2\varphi_{1,11} - 2\varphi_{2,12} - \varphi_{1,22} \\ 2\varphi_{2,22} - 2\varphi_{1,12} - \varphi_{2,11} \\ 0 \\ -\left(3\varphi_{1,11} + 2\varphi_{2,12} + \varphi_{1,22}\right) \\ -\left(3\varphi_{2,22} + 2\varphi_{1,12} + \varphi_{2,11}\right) \\ 4\varphi_{1,22} + 8\varphi_{2,12} - 3\varphi_{1,11} \\ 4\varphi_{2,11} + 8\varphi_{1,12} - 3\varphi_{2,22} \\ 0 \\ 0 \\ 0 \end{Bmatrix},$$

$$\boldsymbol{\eta}^{(3)} = \frac{1}{5}\begin{Bmatrix} 0 \\ 0 \\ -\left(u^0_{3,11} + u^0_{3,22} + \varphi_{1,1} + \varphi_{2,2}\right) \\ 0 \\ 0 \\ 0 \\ 0 \\ 4u^0_{3,11} - u^0_{3,22} + 4\varphi_{1,1} - \varphi_{2,2} \\ 4u^0_{3,22} - u^0_{3,11} + 4\varphi_{2,2} - \varphi_{1,1} \\ 5\left(\varphi_{1,2} + \varphi_{2,1} + 2u^0_{3,12}\right) \end{Bmatrix}, \quad \boldsymbol{\eta}^{(4)} = \frac{1}{5}\begin{Bmatrix} 0 \\ 0 \\ -\left(u^0_{3,11} + u^0_{3,22}\right) \\ 0 \\ 0 \\ 0 \\ 0 \\ 4u^0_{3,11} - u^0_{3,22} \\ 4u^0_{3,22} - u^0_{3,11} \\ 10u^0_{3,12} \end{Bmatrix}, \tag{A.3b}$$

$$\boldsymbol{\eta}^{(5)} = \frac{1}{5}\begin{Bmatrix} 0 \\ 0 \\ -\left(\varphi_{1,1} + \varphi_{2,2}\right) \\ 0 \\ 0 \\ 0 \\ 0 \\ 4\varphi_{1,1} - \varphi_{2,2} \\ 4\varphi_{2,2} - \varphi_{1,1} \\ 5\left(\varphi_{1,2} + \varphi_{2,1}\right) \end{Bmatrix}, \quad \boldsymbol{\eta}^{(6)} = \frac{1}{5}\begin{Bmatrix} -\left(\varphi_1 + u^0_{3,1}\right) \\ -\left(\varphi_2 + u^0_{3,2}\right) \\ 0 \\ 4\left(\varphi_1 + u^0_{3,1}\right) \\ 4\left(\varphi_2 + u^0_{3,2}\right) \\ -\left(\varphi_1 + u^0_{3,1}\right) \\ -\left(\varphi_2 + u^0_{3,2}\right) \\ 0 \\ 0 \\ 0 \end{Bmatrix}.$$

The components of rotation gradients in Eq. (13) are expressed as follows

$$\boldsymbol{\chi}^{(0)} = \frac{1}{2}\begin{Bmatrix} u^0_{3,12} \\ -u^0_{3,12} \\ u^0_{3,22} - u^0_{3,11} \\ 0 \\ u^0_{2,11} - u^0_{1,12} \\ u^0_{2,12} - u^0_{1,22} \end{Bmatrix}, \quad \boldsymbol{\chi}^{(1)} = \frac{1}{2}\begin{Bmatrix} -u^0_{3,12} \\ u^0_{3,12} \\ u^0_{3,11} - u^0_{3,22} \\ 0 \\ 0 \\ 0 \end{Bmatrix}, \quad \boldsymbol{\chi}^{(2)} = \frac{1}{2}\begin{Bmatrix} -\varphi_{2,1} \\ \varphi_{1,2} \\ \varphi_{1,1} - \varphi_{2,2} \\ \varphi_{2,1} - \varphi_{1,2} \\ 0 \\ 0 \end{Bmatrix}, \tag{A.4a}$$

$$\chi^{(3)} = \frac{1}{2}\begin{Bmatrix} 0 \\ 0 \\ 0 \\ 0 \\ -u^0_{3,2} \\ u^0_{3,1} \end{Bmatrix}, \quad \chi^{(4)} = \frac{1}{2}\begin{Bmatrix} 0 \\ 0 \\ 0 \\ 0 \\ -\varphi_2 \\ \varphi_1 \end{Bmatrix}, \quad \chi^{(5)} = \frac{1}{2}\begin{Bmatrix} 0 \\ 0 \\ 0 \\ 0 \\ \varphi_{2,11} - \varphi_{1,12} \\ \varphi_{2,12} - \varphi_{1,22} \end{Bmatrix}. \tag{A.4b}$$

APPENDIX B

The stress resultants of the FGP microplates are expressed in terms of the strains and its gradients as follows

$$\begin{Bmatrix} \mathbf{M}^{(0)}_{\varepsilon} \\ \mathbf{M}^{(1)}_{\varepsilon} \\ \mathbf{M}^{(2)}_{\varepsilon} \\ \mathbf{M}^{(3)}_{\varepsilon} \end{Bmatrix} = \begin{bmatrix} \mathbf{A}^{\varepsilon} & \mathbf{B}^{\varepsilon} & \mathbf{B}^{\varepsilon}_s & \mathbf{0} \\ \mathbf{B}^{\varepsilon} & \mathbf{D}^{\varepsilon} & \mathbf{D}^{\varepsilon}_s & \mathbf{0} \\ \mathbf{B}^{\varepsilon}_s & \mathbf{D}^{\varepsilon}_s & \mathbf{H}^{\varepsilon}_s & \mathbf{0} \\ \mathbf{0} & \mathbf{0} & \mathbf{0} & \mathbf{A}^{\varepsilon}_s \end{bmatrix} \begin{Bmatrix} \boldsymbol{\varepsilon}^{(0)} \\ \boldsymbol{\varepsilon}^{(1)} \\ \boldsymbol{\varepsilon}^{(2)} \\ \boldsymbol{\varepsilon}^{(3)} \end{Bmatrix}, \tag{B.1a}$$

$$\begin{Bmatrix} \mathbf{M}^{(0)}_{x} \\ \mathbf{M}^{(1)}_{x} \\ \mathbf{M}^{(2)}_{x} \\ \mathbf{M}^{(3)}_{x} \\ \mathbf{M}^{(4)}_{x} \\ \mathbf{M}^{(5)}_{x} \end{Bmatrix} = \begin{bmatrix} \mathbf{A}^{x} & \overline{\mathbf{B}}^{x} & \overline{\mathbf{B}}^{x}_s & \overline{\mathbf{B}}^{x} & \overline{\mathbf{B}}^{x}_s & \mathbf{B}^{x}_s \\ \overline{\mathbf{B}}^{x} & \overline{\mathbf{D}}^{x} & \overline{\mathbf{D}}^{x}_s & \overline{\mathbf{E}}^{x} & \overline{\mathbf{E}}^{x}_s & \overline{\mathbf{F}}^{x}_s \\ \overline{\mathbf{B}}^{x}_s & \overline{\mathbf{D}}^{x}_s & \overline{\mathbf{H}}^{x}_s & \overline{\mathbf{G}}^{x}_s & \overline{\mathbf{I}}^{x} & \overline{\mathbf{J}}^{x} \\ \overline{\mathbf{B}}^{x} & \overline{\mathbf{E}}^{x} & \overline{\mathbf{G}}^{x}_s & \overline{\overline{\mathbf{D}}}^{x} & \overline{\overline{\mathbf{D}}}^{x}_s & \overline{\mathbf{K}}^{x}_s \\ \overline{\overline{\mathbf{B}}}^{x}_s & \overline{\mathbf{E}}^{x}_s & \overline{\mathbf{I}}^{x} & \overline{\overline{\mathbf{D}}}^{x}_s & \overline{\overline{\mathbf{H}}}^{x}_s & \overline{\mathbf{L}} \\ \mathbf{B}^{x}_s & \overline{\mathbf{F}}^{x}_s & \overline{\mathbf{J}}^{x} & \overline{\mathbf{K}}^{x}_s & \overline{\mathbf{L}} & \mathbf{H}^{x}_s \end{bmatrix} \begin{Bmatrix} \chi^{(0)} \\ \chi^{(2)} \\ \chi^{(3)} \\ \chi^{(4)} \\ \chi^{(5)} \end{Bmatrix}, \tag{B.1b}$$

$$\begin{Bmatrix} \mathbf{M}^{(0)}_{\eta} \\ \mathbf{M}^{(1)}_{\eta} \\ \mathbf{M}^{(2)}_{\eta} \\ \mathbf{M}^{(3)}_{\eta} \\ \mathbf{M}^{(4)}_{\eta} \\ \mathbf{M}^{(5)}_{\eta} \\ \mathbf{M}^{(6)}_{\eta} \end{Bmatrix} = \begin{bmatrix} \mathbf{A}^{\eta} & \mathbf{B}^{\eta} & \mathbf{B}^{\eta}_s & \mathbf{A}^{\eta}_s & \overline{\mathbf{B}}^{\eta} & \overline{\mathbf{B}}^{\eta}_s & \overline{\mathbf{A}}^{\eta}_s \\ \mathbf{B}^{\eta} & \mathbf{D}^{\eta} & \mathbf{D}^{\eta}_s & \mathbf{D}^{\eta}_{ts} & \overline{\mathbf{O}}^{\eta} & \overline{\mathbf{P}}^{\eta}_s & \overline{\mathbf{Q}}^{\eta}_s \\ \mathbf{B}^{\eta}_s & \mathbf{D}^{\eta}_s & \mathbf{H}^{\eta}_s & \mathbf{D}^{\eta}_{hs} & \overline{\mathbf{F}}^{\eta}_s & \overline{\mathbf{J}}^{\eta} & \overline{\mathbf{F}}^{\eta}_{hs} \\ \mathbf{A}^{\eta}_s & \mathbf{D}^{\eta}_{ts} & \mathbf{D}^{\eta}_{hs} & \mathbf{H}^{\eta}_{ts} & \overline{\mathbf{F}}^{\eta}_{ts} & \overline{\mathbf{J}}^{\eta}_{hs} & \overline{\mathbf{R}}^{\eta} \\ \overline{\mathbf{B}}^{\eta} & \overline{\mathbf{O}}^{\eta} & \overline{\mathbf{F}}^{\eta}_s & \overline{\mathbf{F}}^{\eta}_{ts} & \overline{\mathbf{D}}^{\eta} & \overline{\mathbf{D}}^{\eta}_s & \overline{\mathbf{D}}^{\eta}_{ts} \\ \overline{\mathbf{B}}^{\eta}_s & \overline{\mathbf{P}}^{\eta}_s & \overline{\mathbf{J}}^{\eta} & \overline{\mathbf{J}}^{\eta}_{hs} & \overline{\mathbf{D}}^{\eta}_s & \overline{\mathbf{H}}^{\eta}_s & \overline{\mathbf{D}}^{\eta}_{hs} \\ \overline{\mathbf{A}}^{\eta}_s & \overline{\mathbf{Q}}^{\eta}_s & \overline{\mathbf{F}}^{\eta}_{hs} & \overline{\mathbf{R}}^{\eta} & \overline{\mathbf{D}}^{\eta}_{ts} & \overline{\mathbf{D}}^{\eta}_{hs} & \overline{\mathbf{H}}^{\eta}_{ts} \end{bmatrix} \begin{Bmatrix} \boldsymbol{\eta}^{(0)} \\ \boldsymbol{\eta}^{(1)} \\ \boldsymbol{\eta}^{(2)} \\ \boldsymbol{\eta}^{(3)} \\ \boldsymbol{\eta}^{(4)} \\ \boldsymbol{\eta}^{(5)} \\ \boldsymbol{\eta}^{(6)} \end{Bmatrix}, \tag{B.1c}$$

$$\begin{Bmatrix} \mathbf{M}^{(0)}_{\xi} \\ \mathbf{M}^{(1)}_{\xi} \\ \mathbf{M}^{(2)}_{\xi} \\ \mathbf{M}^{(3)}_{\xi} \\ \mathbf{M}^{(4)}_{\xi} \end{Bmatrix} \begin{bmatrix} \mathbf{A}^{\xi} & \mathbf{B}^{\xi} & \mathbf{B}^{\xi}_s & \overline{\mathbf{B}}^{\xi} & \overline{\mathbf{B}}^{\xi}_s \\ \mathbf{B}^{\xi} & \mathbf{D}^{\xi} & \mathbf{D}^{\xi}_s & \overline{\mathbf{O}}^{\xi} & \overline{\mathbf{P}}^{\xi}_s \\ \mathbf{B}^{\xi}_s & \mathbf{D}^{\xi}_s & \mathbf{H}^{\xi}_s & \overline{\mathbf{F}}^{\xi}_s & \overline{\mathbf{J}}^{\xi} \\ \overline{\mathbf{B}}^{\xi} & \overline{\mathbf{O}}^{\xi} & \overline{\mathbf{F}}^{\xi}_s & \overline{\mathbf{D}}^{\xi} & \overline{\mathbf{D}}^{\xi}_s \\ \overline{\mathbf{B}}^{\xi}_s & \overline{\mathbf{P}}^{\xi}_s & \overline{\mathbf{J}}^{\xi} & \overline{\mathbf{D}}^{\xi}_s & \overline{\mathbf{H}}^{\xi}_s \end{bmatrix} \begin{Bmatrix} \boldsymbol{\xi}^{(0)} \\ \boldsymbol{\xi}^{(1)} \\ \boldsymbol{\xi}^{(2)} \\ \boldsymbol{\xi}^{(3)} \\ \boldsymbol{\xi}^{(4)} \end{Bmatrix}, \tag{B.1d}$$

where the stiffness components of the FGP microplates are defined as follows

$$
\begin{aligned}
&(\mathbf{A}^{\varepsilon},\mathbf{B}^{\varepsilon},\mathbf{D}^{\varepsilon},\mathbf{H}_{s}^{\varepsilon},\mathbf{B}_{s}^{\varepsilon},\mathbf{D}_{s}^{\varepsilon})=\int_{-h/2}^{h/2}\left(1,\Phi_{1},\Phi_{1}^{2},\Phi_{2}^{2},\Phi_{2},\Phi_{1}\Phi_{2}\right)\mathbf{Q}_{\varepsilon}^{(i)}\mathrm{d}x_{3},\quad \mathbf{A}_{s}^{\varepsilon}=\int_{-h/2}^{h/2}\Phi_{3}^{2}\mathbf{Q}_{\varepsilon}^{(o)}\mathrm{d}x_{3},\\
&\left(\mathbf{A}^{\xi},\mathbf{B}^{\xi},\mathbf{B}_{s}^{\xi},\overline{\mathbf{B}}^{\xi},\overline{\mathbf{B}}_{s}^{\xi}\right)=\left(A^{\xi},B^{\xi},B_{s}^{\xi},\overline{B}^{\xi},\overline{B}_{s}^{\xi}\right)\mathbf{I}_{3\times3}=\int_{-h/2}^{h/2}\left(1,\Phi_{1},\Phi_{2},\Phi_{1,3},\Phi_{2,3}\right)\alpha_{\xi}\mathbf{I}_{3\times3}\mathrm{d}x_{3},\\
&\left(\mathbf{D}^{\xi},\mathbf{D}_{s}^{\xi},\overline{\mathbf{O}}^{\xi},\overline{\mathbf{P}}_{s}^{\xi}\right)=\left(D^{\xi},D_{s}^{\xi},\overline{O}^{\xi},\overline{P}_{s}^{\xi}\right)\mathbf{I}_{3\times3}=\int_{-h/2}^{h/2}\Phi_{1}\left(\Phi_{1},\Phi_{2},\Phi_{1,3},\Phi_{2,3}\right)\alpha_{\xi}\mathbf{I}_{3\times3}\mathrm{d}x_{3},\\
&\left(\mathbf{H}_{s}^{\xi},\overline{\mathbf{F}}_{s}^{\xi},\overline{\mathbf{J}}^{\xi},\overline{\mathbf{D}}^{\xi},\overline{\mathbf{D}}_{s}^{\xi},\overline{\mathbf{H}}_{s}^{\xi}\right)=\left(H_{s}^{\xi},\overline{F}_{s}^{\xi},\overline{J}^{\xi},\overline{D}^{\xi},\overline{D}_{s}^{\xi},\overline{H}_{s}^{\xi}\right)\mathbf{I}_{3\times3}=\int_{-h/2}^{h/2}\left(\Phi_{2}^{2},\Phi_{2}\Phi_{1,3},\Phi_{2}\Phi_{2,3},\Phi_{1,3}^{2},\Phi_{1,3}\Phi_{2,3},\Phi_{2,3}^{2}\right)\alpha_{\xi}\mathbf{I}_{3\times3}\mathrm{d}x_{3},\\
&\left(\mathbf{A}^{\eta},\mathbf{B}^{\eta},\mathbf{B}_{s}^{\eta},\mathbf{A}_{s}^{\eta},\overline{\mathbf{B}}^{\eta},\overline{\mathbf{B}}_{s}^{\eta},\overline{\mathbf{A}}_{s}^{\eta}\right)=\left(A^{\eta},B^{\eta},B_{s}^{\eta},A_{s}^{\eta},\overline{B}^{\eta},\overline{B}_{s}^{\eta},\overline{A}_{s}^{\eta}\right)\mathbf{I}_{10\times10}=\int_{-h/2}^{h/2}\left(1,\Phi_{1},\Phi_{2},\Phi_{3},\Phi_{1,3},\Phi_{2,3},\Phi_{3,3}\right)\alpha_{\eta}\mathbf{I}_{10\times10}\mathrm{d}x_{3},\\
&\left(\mathbf{D}^{\eta},\mathbf{D}_{s}^{\eta},\mathbf{D}_{ts}^{\eta},\overline{\mathbf{O}}^{\eta},\overline{\mathbf{P}}_{s}^{\eta},\overline{\mathbf{Q}}_{s}^{\eta}\right)=\left(D^{\eta},D_{s}^{\eta},D_{ts}^{\eta},\overline{O}^{\eta},\overline{P}_{s}^{\eta},\overline{Q}_{s}^{\eta}\right)\mathbf{I}_{10\times10}=\int_{-h/2}^{h/2}\Phi_{1}\left(\Phi_{1},\Phi_{2},\Phi_{3},\Phi_{1,3},\Phi_{2,3},\Phi_{3,3}\right)\alpha_{\eta}\mathbf{I}_{10\times10}\mathrm{d}x_{3},\\
&\left(\mathbf{H}_{s}^{\eta},\overline{\mathbf{D}}_{hs}^{\eta},\overline{\mathbf{F}}_{s}^{\eta},\overline{\mathbf{J}}^{\eta},\overline{\mathbf{F}}_{hs}^{\eta}\right)=\left(H_{s}^{\eta},\overline{D}_{hs}^{\eta},\overline{F}_{s}^{\eta},\overline{J}^{\eta},\overline{F}_{hs}^{\eta}\right)\mathbf{I}_{10\times10}=\int_{-h/2}^{h/2}\Phi_{2}\left(\Phi_{2},\Phi_{3},\Phi_{1,3},\Phi_{2,3},\Phi_{3,3}\right)\alpha_{\eta}\mathbf{I}_{10\times10}\mathrm{d}x_{3},\\
&\left(\mathbf{H}_{ts}^{\eta},\overline{\mathbf{F}}_{ts}^{\eta},\overline{\mathbf{J}}_{hs}^{\eta},\overline{\mathbf{R}}^{\eta}\right)=\left(H_{ts}^{\eta},\overline{F}_{ts}^{\eta},\overline{J}_{hs}^{\eta},\overline{R}^{\eta}\right)\mathbf{I}_{10\times10}=\int_{-h/2}^{h/2}\Phi_{3}\left(\Phi_{3},\Phi_{1,3},\Phi_{2,3},\Phi_{3,3}\right)\alpha_{\eta}\mathbf{I}_{10\times10}\mathrm{d}x_{3},\\
&\left(\overline{\mathbf{D}}^{\eta},\overline{\mathbf{D}}_{s}^{\eta},\overline{\mathbf{D}}_{ts}^{\eta},\overline{\mathbf{H}}_{s}^{\eta},\overline{\mathbf{D}}_{hs}^{\eta},\overline{\mathbf{H}}_{ts}^{\eta}\right)=\left(\overline{D}^{\eta},\overline{D}_{s}^{\eta},\overline{D}_{ts}^{\eta},\overline{H}_{s}^{\eta},\overline{D}_{hs}^{\eta},\overline{H}_{ts}^{\eta}\right)\mathbf{I}_{10\times10}\\
&\qquad=\int_{-h/2}^{h/2}\left(\Phi_{1,3}^{2},\Phi_{1,3}\Phi_{2,3},\Phi_{1,3}\Phi_{3,3},\Phi_{2,3}^{2},\Phi_{2,3}\Phi_{3,3},\Phi_{3,3}^{2}\right)\alpha_{\eta}\mathbf{I}_{10\times10}\mathrm{d}x_{3},\\
&\left(\mathbf{A}^{\chi},\overline{\mathbf{B}}^{\chi},\overline{\mathbf{B}}_{s}^{\chi},\overline{\overline{\mathbf{B}}}^{\chi},\overline{\overline{\mathbf{B}}}_{s}^{\chi},\mathbf{B}_{s}^{\chi}\right)=\left(A^{\chi},\overline{B}^{\chi},\overline{B}_{s}^{\chi},\overline{\overline{B}}^{\chi},\overline{\overline{B}}_{s}^{\chi},B_{s}^{\chi}\right)\mathbf{I}_{6\times6}=\int_{-h/2}^{h/2}\left(1,\Phi_{1,3},\Phi_{2,3},\Phi_{1,33},\Phi_{2,33},\Phi_{2}\right)\alpha_{\chi}\mathbf{I}_{6\times6}\mathrm{d}x_{3},\\
&\left(\overline{\mathbf{D}}^{\chi},\overline{\mathbf{D}}_{s}^{\chi},\overline{\mathbf{E}}^{\chi},\overline{\mathbf{E}}_{s}^{\chi},\overline{\mathbf{F}}_{s}^{\chi}\right)=\left(\overline{D}^{\chi},\overline{D}_{s}^{\chi},\overline{E}^{\chi},\overline{E}_{s}^{\chi},\overline{F}_{s}^{\chi}\right)\mathbf{I}_{6\times6}=\int_{-h/2}^{h/2}\Phi_{1,3}\left(\Phi_{1,3},\Phi_{2,3},\Phi_{1,33},\Phi_{2,33},\Phi_{2}\right)\alpha_{\chi}\mathbf{I}_{6\times6}\mathrm{d}x_{3},\\
&\left(\overline{\mathbf{H}}_{s}^{\chi},\overline{\mathbf{G}}_{s}^{\chi},\overline{\mathbf{I}}^{\chi},\overline{\mathbf{J}}^{\chi}\right)=\left(\overline{H}_{s}^{\chi},\overline{G}_{s}^{\chi},\overline{I}^{\chi},\overline{J}^{\chi}\right)\mathbf{I}_{6\times6}=\int_{-h/2}^{h/2}\Phi_{2,3}\left(\Phi_{2,3},\Phi_{1,33},\Phi_{2,33},\Phi_{2}\right)\alpha_{\chi}\mathbf{I}_{6\times6}\mathrm{d}x_{3},\\
&\left(\overline{\overline{\mathbf{D}}}^{\chi},\overline{\overline{\mathbf{D}}}_{s}^{\chi},\overline{\mathbf{K}}_{s}^{\chi},\overline{\overline{\mathbf{H}}}_{s}^{\chi},\overline{\mathbf{L}}^{\chi},\mathbf{H}_{s}^{\chi}\right)=\left(\overline{\overline{D}}^{\chi},\overline{\overline{D}}_{s}^{\chi},\overline{K}_{s}^{\chi},\overline{\overline{H}}_{s}^{\chi},\overline{L}^{\chi},H_{s}^{\chi}\right)\mathbf{I}_{6\times6}\\
&\qquad=\int_{-h/2}^{h/2}\left(\Phi_{1,33}^{2},\Phi_{1,33}\Phi_{2,33},\Phi_{1,33}\Phi_{2},\Phi_{2,33}^{2},\Phi_{2,33}\Phi_{2},\Phi_{2}^{2}\right)\alpha_{\chi}\mathbf{I}_{6\times6}\mathrm{d}x_{3}.
\end{aligned}
\tag{B.2}
$$

APPENDIX C

The components of stiffness matrix $\mathbf{K}^{\xi}$, $\mathbf{K}^{\eta}$ and load vector $\mathbf{F}$ are defined as follows

$$
\begin{aligned}
K_{ijkl}^{\xi11}&=A^{\xi}\left(T_{ik}^{33}S_{jl}^{00}+T_{ik}^{22}S_{jl}^{11}\right),\quad K_{ijkl}^{\xi12}=A^{\xi}\left(T_{ik}^{13}S_{jl}^{20}+T_{ik}^{02}S_{jl}^{31}\right),\\
K_{ijkl}^{\xi13}&=B^{\xi}\left(T_{ik}^{33}S_{jl}^{00}+T_{ik}^{13}S_{jl}^{20}+T_{ik}^{02}S_{jl}^{31}+T_{ik}^{22}S_{jl}^{11}\right),\\
K_{ijkl}^{\xi14}&=B_{s}^{\xi}\left(T_{ik}^{33}S_{jl}^{00}+T_{ik}^{22}S_{jl}^{11}\right),\quad K_{ijkl}^{\xi15}=B_{s}^{\xi}\left(T_{ik}^{13}S_{jl}^{20}+T_{ik}^{02}S_{jl}^{31}\right),\\
K_{ijkl}^{\xi22}&=A^{\xi}\left(T_{ik}^{11}S_{jl}^{22}+T_{ik}^{00}S_{jl}^{33}\right),\quad K_{ijkl}^{\xi23}=B^{\xi}\left(T_{ik}^{31}S_{jl}^{02}+T_{ik}^{11}S_{jl}^{22}+T_{ik}^{20}S_{jl}^{13}+T_{ik}^{00}S_{jl}^{33}\right),\\
K_{ijkl}^{\xi24}&=B_{s}^{\xi}\left(T_{ik}^{31}S_{jl}^{02}+T_{ik}^{20}S_{jl}^{13}\right),\quad K_{ijkl}^{\xi25}=B_{s}^{\xi}\left(T_{ik}^{11}S_{jl}^{22}+T_{ik}^{00}S_{jl}^{33}\right),\\
K_{ijkl}^{\xi33}&=D^{\xi}\left(T_{ik}^{33}S_{jl}^{00}+T_{ik}^{00}S_{jl}^{33}+T_{ik}^{31}S_{jl}^{02}+T_{ik}^{02}S_{jl}^{31}+T_{ik}^{13}S_{jl}^{20}+T_{ik}^{20}S_{jl}^{13}+T_{ik}^{11}S_{jl}^{22}+T_{ik}^{22}S_{jl}^{11}\right)\\
&\quad+\overline{D}^{\xi}\left(T_{ik}^{22}S_{jl}^{00}+T_{ik}^{20}S_{jl}^{02}+T_{ik}^{02}S_{jl}^{20}+T_{ik}^{00}S_{jl}^{22}\right),\\
K_{ijkl}^{\xi34}&=D_{s}^{\xi}\left(T_{ik}^{33}S_{jl}^{00}+T_{ik}^{31}S_{jl}^{02}+T_{ik}^{22}S_{jl}^{11}+T_{ik}^{20}S_{jl}^{13}\right)+\overline{D}_{s}^{\xi}\left(T_{ik}^{22}S_{jl}^{00}+T_{ik}^{20}S_{jl}^{02}\right),\\
K_{ijkl}^{\xi35}&=D_{s}^{\xi}\left(T_{ik}^{13}S_{jl}^{20}+T_{ik}^{11}S_{jl}^{22}+T_{ik}^{02}S_{jl}^{31}+T_{ik}^{00}S_{jl}^{33}\right)+\overline{D}_{s}^{\xi}\left(T_{ik}^{02}S_{jl}^{20}+T_{ik}^{00}S_{jl}^{22}\right),\\
K_{ijkl}^{\xi44}&=H_{s}^{\xi}T_{ik}^{33}S_{jl}^{00}+H_{s}^{\xi}T_{ik}^{22}S_{jl}^{11}+\overline{H}_{s}^{\xi}T_{ik}^{22}S_{jl}^{00},\quad K_{ijkl}^{\xi45}=H_{s}^{\xi}T_{ik}^{13}S_{jl}^{20}+H_{s}^{\xi}T_{ik}^{02}S_{jl}^{31}+\overline{H}_{s}^{\xi}T_{ik}^{02}S_{jl}^{20},\\
K_{ijkl}^{\xi55}&=H_{s}^{\xi}T_{ik}^{00}S_{jl}^{33}+H_{s}^{\xi}T_{ik}^{11}S_{jl}^{22}+\overline{H}_{s}^{\xi}T_{ik}^{00}S_{jl}^{22},
\end{aligned}
\tag{C.1a}
$$

$$
\begin{aligned}
K_{ijkl}^{\eta 11} &= A^{\eta}\left(22T_{ik}^{33}S_{jl}^{00}-11T_{ik}^{31}S_{jl}^{02}-11T_{ik}^{13}S_{jl}^{20}+18T_{ik}^{11}S_{jl}^{22}+72T_{ik}^{22}S_{jl}^{11}\right)/25,\\
K_{ijkl}^{\eta 12} &= 2A^{\eta}\left(-11T_{ik}^{13}S_{jl}^{20}-11T_{ik}^{02}S_{jl}^{31}+18T_{ik}^{11}S_{jl}^{22}+18T_{ik}^{22}S_{jl}^{11}\right)/25,\\
K_{ijkl}^{\eta 13} &= B^{\eta}\left(22T_{ik}^{33}S_{jl}^{00}-11T_{ik}^{31}S_{jl}^{02}-33T_{ik}^{13}S_{jl}^{20}+54T_{ik}^{11}S_{jl}^{22}-22T_{ik}^{02}S_{jl}^{31}+108T_{ik}^{22}S_{jl}^{11}\right)/25,\\
K_{ijkl}^{\eta 25} &= B_{s}^{\eta}\left(72T_{ik}^{11}S_{jl}^{22}+22T_{ik}^{00}S_{jl}^{33}-11T_{ik}^{02}S_{jl}^{31}-11T_{ik}^{20}S_{jl}^{13}+18T_{ik}^{22}S_{jl}^{11}\right)/25-\overline{A}_{s}^{\eta}\left(7T_{ik}^{02}S_{jl}^{11}+11T_{ik}^{00}S_{jl}^{13}\right)/25,\\
K_{ijkl}^{\eta 33} &= D^{\eta}\left(22T_{ik}^{33}S_{jl}^{00}-33T_{ik}^{31}S_{jl}^{02}-33T_{ik}^{13}S_{jl}^{20}+162T_{ik}^{11}S_{jl}^{22}+162T_{ik}^{22}S_{jl}^{11}+22T_{ik}^{00}S_{jl}^{33}-33T_{ik}^{02}S_{jl}^{31}-33T_{ik}^{20}S_{jl}^{13}\right)/25,\\
&\quad-\overline{Q}_{s}^{\eta}\left(11T_{ik}^{00}S_{jl}^{13}+11T_{ik}^{13}S_{jl}^{00}+11T_{ik}^{31}S_{jl}^{00}+11T_{ik}^{00}S_{jl}^{31}+21T_{ik}^{02}S_{jl}^{11}+21T_{ik}^{11}S_{jl}^{02}+21T_{ik}^{11}S_{jl}^{20}+21T_{ik}^{20}S_{jl}^{11}\right)/25,\\
&\quad+\left(H_{ts}^{\eta}+2\overline{F}_{ts}^{\eta}+\overline{D}^{\eta}\right)\left(18T_{ik}^{22}S_{jl}^{00}-7T_{ik}^{20}S_{jl}^{02}-7T_{ik}^{02}S_{jl}^{20}+18T_{ik}^{00}S_{jl}^{22}+100T_{ik}^{11}S_{jl}^{11}\right)/25+18\overline{H}_{ts}^{\eta}\left(T_{ik}^{11}S_{jl}^{00}+T_{ik}^{00}S_{jl}^{11}\right)/25,\\
K_{ijkl}^{\eta 34} &= D_{s}^{\eta}\left(22T_{ik}^{33}S_{jl}^{00}-33T_{ik}^{31}S_{jl}^{02}-11T_{ik}^{13}S_{jl}^{20}+54T_{ik}^{11}S_{jl}^{22}-22T_{ik}^{20}S_{jl}^{13}+108T_{ik}^{22}S_{jl}^{11}\right)/25\\
&\quad-\overline{Q}_{s}^{\eta}\left(11T_{ik}^{13}S_{jl}^{00}+21T_{ik}^{11}S_{jl}^{02}\right)/25+\left(H_{ts}^{\eta}+\overline{J}_{hs}^{\eta}+\overline{F}_{ts}^{\eta}+\overline{D}_{s}^{\eta}\right)\left(18T_{ik}^{22}S_{jl}^{00}-7T_{ik}^{20}S_{jl}^{02}+50T_{ik}^{11}S_{jl}^{11}\right)/25\\
&\quad-\overline{F}_{hs}^{\eta}\left(14T_{ik}^{20}S_{jl}^{11}+11T_{ik}^{31}S_{jl}^{00}+7T_{ik}^{11}S_{jl}^{20}\right)/25+18\overline{H}_{is}^{\eta}T_{ik}^{11}S_{jl}^{00}/25,\\
K_{ijkl}^{\eta 35} &= D_{s}^{\eta}\left(108T_{ik}^{11}S_{jl}^{22}+54T_{ik}^{22}S_{jl}^{11}+22T_{ik}^{00}S_{jl}^{33}-33T_{ik}^{02}S_{jl}^{31}-11T_{ik}^{20}S_{jl}^{13}-22T_{ik}^{13}S_{jl}^{20}\right)/25\\
&\quad-\overline{Q}_{s}^{\eta}\left(21T_{ik}^{02}S_{jl}^{11}+11T_{ik}^{00}S_{jl}^{13}\right)/25+\left(H_{ts}^{\eta}+\overline{J}_{hs}^{\eta}+\overline{F}_{ts}^{\eta}+\overline{D}_{s}^{\eta}\right)\left(18T_{ik}^{00}S_{jl}^{22}-7T_{ik}^{02}S_{jl}^{20}+50T_{ik}^{11}S_{jl}^{11}\right)/25\\
&\quad-\overline{F}_{hs}^{\eta}\left(14T_{ik}^{11}S_{jl}^{20}+11T_{ik}^{00}S_{jl}^{31}+7T_{ik}^{20}S_{jl}^{11}\right)/25+18\overline{H}_{is}^{\eta}T_{ik}^{00}S_{jl}^{11}/25,\\
K_{ijkl}^{\eta 44} &= H_{s}^{\eta}\left(22T_{ik}^{33}S_{jl}^{00}-11T_{ik}^{31}S_{jl}^{02}-11T_{ik}^{13}S_{jl}^{20}+18T_{ik}^{11}S_{jl}^{22}+72T_{ik}^{22}S_{jl}^{11}\right)/25+18\overline{H}_{is}^{\eta}T_{ik}^{11}S_{jl}^{00}/25\\
&\quad+\left(H_{is}^{\eta}+2\overline{J}_{hs}^{\eta}+\overline{H}_{s}^{\eta}\right)\left(18T_{ik}^{22}S_{jl}^{00}+25T_{ik}^{11}S_{jl}^{11}\right)-\overline{F}_{hs}^{\eta}\left(11T_{ik}^{31}S_{jl}^{00}+7T_{ik}^{11}S_{jl}^{20}+11T_{ik}^{13}S_{jl}^{00}+7T_{ik}^{11}S_{jl}^{02}\right)/25,\\
K_{ijkl}^{\eta 45} &= H_{s}^{\eta}\left(36T_{ik}^{11}S_{jl}^{22}+36T_{ik}^{22}S_{jl}^{11}-22T_{ik}^{13}S_{jl}^{20}-22T_{ik}^{02}S_{jl}^{31}\right)/25-14\overline{F}_{hs}^{\eta}\left(T_{ik}^{02}S_{jl}^{11}+T_{ik}^{11}S_{jl}^{20}\right)/25\\
&\quad+\left(H_{ts}^{\eta}+2\overline{J}_{hs}^{\eta}+\overline{H}_{s}^{\eta}\right)\left(25T_{ik}^{11}S_{jl}^{11}-7T_{ik}^{02}S_{jl}^{20}\right)/25,\\
K_{ijkl}^{\eta 55} &= H_{s}^{\eta}\left(72T_{ik}^{11}S_{jl}^{22}+22T_{ik}^{00}S_{jl}^{33}-11T_{ik}^{02}S_{jl}^{31}-11T_{ik}^{20}S_{jl}^{13}+18T_{ik}^{22}S_{jl}^{11}\right)/25+18\overline{H}_{ts}^{\eta}T_{ik}^{00}S_{jl}^{11}/25\\
&\quad+\left(H_{ts}^{\eta}+2\overline{J}_{hs}^{\eta}+\overline{H}_{s}^{\eta}\right)\left(18T_{ik}^{00}S_{jl}^{22}+25T_{ik}^{11}S_{jl}^{11}\right)/25-\overline{F}_{hs}^{\eta}\left(11T_{ik}^{00}S_{jl}^{13}+7T_{ik}^{02}S_{jl}^{11}+11T_{ik}^{00}S_{jl}^{31}+7T_{ik}^{20}S_{jl}^{11}\right)/25,
\end{aligned}
\tag{C.1b}
$$

$$
f_{ij}=\int_{0}^{a}\int_{0}^{b}qX_{i}Y_{j}\mathrm{d}x_{1}\mathrm{d}x_{2},
\tag{C.1c}
$$

$$
T_{ik}^{rs}=\int_{0}^{a}\frac{\partial^{r}R_{i}}{\partial x_{1}^{r}}\frac{\partial^{s}R_{k}}{\partial x_{1}^{s}}\mathrm{d}x_{1},\qquad S_{jl}^{rs}=\int_{0}^{a}\frac{\partial^{r}P_{j}}{\partial x_{2}^{r}}\frac{\partial^{s}P_{l}}{\partial x_{2}^{s}}\mathrm{d}x_{2}.
\tag{C.1d}
$$